PCCP

ROYAL SOCIETY OF CHEMISTRY

PAPER

View Article Online
View Journal | View Issue

Check for updates

Cite this: *Phys. Chem. Chem. Phys.*, 2024, **26**, 5081

Accelerated acquisition of wideline solid-state NMR spectra of spin 3/2 nuclei by frequency-stepped indirect detection experiments†

Sujeewa N. S. Lamahewage,[ab] Benjamin A. Atterberry,[ab] Rick W. Dorn,[ab] Eunbyeol Gi,[ab] Maxwell R. Kimball,[c] Janet Blümel,*[c] Javier Vela[ab] and Aaron J. Rossini*[ab]

Received 18th October 2023,
Accepted 15th January 2024

DOI: 10.1039/d3cp05055f

rsc.li/pccp

73% of all NMR-active nuclei are quadrupolar nuclei with a nuclear spin $I > 1/2$. The broadening of the solid-state NMR signals by the quadrupolar interaction often leads to poor sensitivity and low resolution. In this work we present experimental and theoretical investigations of magic angle spinning (MAS) ^{1}H{X} double-echo resonance-echo saturation-pulse double-resonance (DE-RESPDOR) and Y{X} *J*-resolved solid-state NMR experiments for the indirect detection of spin 3/2 quadrupolar nuclei (X = spin 3/2 nuclei, Y = spin 1/2 nuclei). In these experiments, the spectrum of the quadrupolar nucleus is reconstructed by plotting the observed dephasing of the detected spin as a function of the transmitter offset of the indirectly detected spin. Numerical simulations were used to investigate the achievable levels of dephasing and to predict the lineshapes of indirectly detected NMR spectra of the quadrupolar nucleus. We demonstrate ^{1}H, ^{31}P and ^{207}Pb detection of ^{35}Cl, ^{81}Br, and ^{63}Cu (I = 3/2) nuclei in *trans*-$Cl_2Pt(NH_3)_2$ (transplatin), $(CH_3NH_3)PbCl_3$ (methylammonium lead chloride, $MAPbCl_3$), $(CH_3NH_3)PbBr_3$ (methylammonium lead bromide, $MAPbBr_3$) and $CH_3C(CH_2PPh_2)_3CuI$ (1,1,1-tris(diphenylphosphinomethyl)ethane copper(I) iodide, triphosCuI), respectively. In all of these experiments, we were able to detect megahertz wide central transition or satellite transition powder patterns. Significant time savings and gains in sensitivity were attained in several test cases. Additionally, the indirect detection experiments provide valuable structural information because they confirm the presence of dipolar or scalar couplings between the detected nucleus and the quadrupolar nucleus of interest. Finally, numerical simulations suggest these methods are also potentially applicable to abundant spin 5/2 and spin 7/2 quadrupolar nuclei.

Open Access Article. Published on 16 January 2024. Downloaded on 2/10/2026 6:49:38 PM.
This article is licensed under a Creative Commons Attribution-NonCommercial 3.0 Unported Licence.

Introduction

High-resolution magic angle spinning (MAS) solid-state nuclear magnetic resonance spectroscopy has played a pivotal role in determining the molecular structure and dynamics of inorganic materials, organic solids, and biomolecules within crystalline and amorphous systems.[1–3] However, many NMR-active nuclei remain understudied due to technical difficulties in recording or interpreting their NMR spectra. For example, low natural abundances, low gyromagnetic ratios, large nuclear electric quadrupole moments (Q), long spin–lattice relaxation time constants (particularly for spin 1/2 nuclei), or some combination of these properties make acquisition of solid-state NMR spectra challenging.[4] Approximately 73% of all NMR-active isotopes are quadrupolar nuclei, with the vast majority having half-integer spins (I = 3/2, 5/2, 7/2, or 9/2).[5] Quadrupolar nuclei often give rise to extremely broad solid-state NMR spectra due to the first and second order quadrupolar interactions. When the second order quadrupolar interaction (SOQI) is sizable, only the central transition (CT) is typically observable, and the satellite transitions (ST) are usually broadened beyond detection. In such cases, the NMR spectrum of the central transition could be several megahertz broad, necessitating the use of wideline solid-state NMR techniques.[6–9]

Slichter first reported the frequency-stepped acquisition of wideline solid-state NMR spectra for ^{195}Pt (I = 1/2) by recording the intensity of Hahn echoes at variable frequency offsets.[10] Following this work, additional wideline NMR studies on half-integer quadrupolar nuclei were performed for nuclei such as

[a] *US Department of Energy, Ames National Laboratory, Ames, Iowa, 50011, USA. E-mail: arossini@iastate.edu; Tel: +1-515-294-8952*
[b] *Iowa State University, Department of Chemistry, Ames, IA, 50011, USA*
[c] *Texas A&M University, Department of Chemistry, College Station, Texas, 77842, USA. E-mail: bluemel@tamu.edu; Tel: +1-979-845-7749*

† Electronic supplementary information (ESI) available: Shows additional solid-state NMR spectroscopy spectra, PXRD patterns and numerical simulations. Raw NMR data associated and SIMPSON simulation files associated with the main text figures are available for download at DOI: **https://doi.org/10.5281/zenodo.10014989**. The CCDC 2250183 contains the supplementary crystallographic data for the copper complex $CH_3C(CH_2PPh_2)_3CuI$ (triphosCuI) for this paper. For ESI and crystallographic data in CIF or other electronic format see DOI: **https://doi.org/10.1039/d3cp05055f**

Open Access Article. Published on 16 January 2024. Downloaded on 2/10/2026 6:49:38 PM.
This article is licensed under a Creative Commons Attribution-NonCommercial 3.0 Unported Licence.

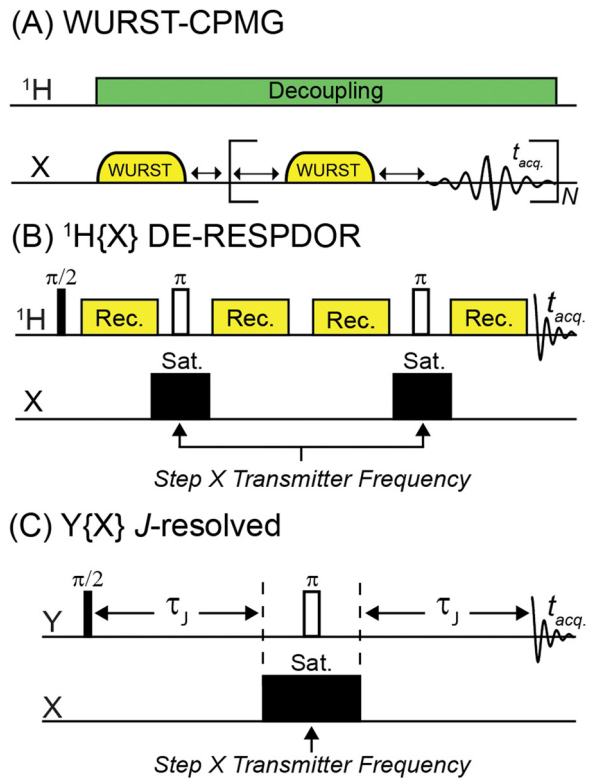

Fig. 1 Pulse sequences used in this work. (A) WURST-CPMG pulse sequence used for direct detection of ^{35}Cl and ^{81}Br solid-state NMR spectra. (B) ^{1}H{X} DE-RESPDOR pulse sequence used for indirect detection of ^{35}Cl and ^{81}Br. (C) Y{X} Heteronuclear spin echo (*J*-resolved) pulse sequence used for ^{207}Pb{^{35}Cl} and ^{31}P{^{63}Cu} NMR experiments. The frequency of the saturation pulse(s) in the DE-RESPDOR or *J*-resolved experiments can be varied in order to map the frequency dependence of the dephasing and reconstruct the solid-state NMR spectrum of the indirectly detected spin 3/2 nucleus. Phase cycles for pulse sequences are given in Table S1 (ESI†).

^{91}Zr,[11,12] $^{69/71}$Ga,[9] and ^{59}Co.[8] More recently, the quadrupolar Carr–Purcell–Meiboom–Gill (QCPMG) pulse sequence has found widespread application for acquisition of solid-state NMR spectra of nuclei such as ^{87}Rb and ^{59}Co,[13,14] and low-γ quadrupolar metal nuclei such as ^{67}Zn,[15,16] ^{95}Mo,[17] ^{14}N,[18] ^{91}Zr,[18,19] ^{39}K, ^{25}Mg, and ^{87}Sr.[13,14] CPMG techniques have also been used to probe halogens like $^{35/37}$Cl (I = 3/2),[20] ^{127}I (I = 5/2),[21] and ^{79}Br (I = 3/2)[22] in organic and inorganic materials.[23] O'Dell and Schurko introduced the Wideband Uniform Rate Smooth Truncation (WURST)-QCPMG pulse sequence (Fig. 1A) and used it to obtain wideline solid-state NMR spectra of a variety of quadrupolar nuclei.[6,19,24] WURST-CPMG offers improved excitation and refocusing bandwidths as compared to conventional QCPMG experiments with rectangular excitation and refocusing pulses.

Unfortunately, direct detection wideline solid-state NMR methods often suffer from inadequate sensitivity and long measurement times.[8,11–15,17,22,25,26] An alternative to these direct detection methods is to use indirect detection experiments where the NMR signal from a sensitive "spy nucleus" that offers a narrow linewidth and/or high sensitivity is exploited. Indirect detection has been applied to a variety of quadrupolar nuclei. There are two ways of performing indirect detection. In the first approach, a standard two-dimensional (2D) NMR experiment is performed where a series of 1D NMR spectra are acquired with incrementation of the indirect dimension evolution time delay (t_1). Fourier transformation of the indirect dimension time domain free induction decay yields the spectrum of the indirectly detected nucleus. For example, Gan and Bodenhausen *et al.* independently demonstrated the use of Heteronuclear Multiple Quantum Correlation (HMQC) pulse sequences[27] for the indirect detection of ^{14}N MAS quadrupolar powder patterns by ^{13}C.[28–30] With the advent of fast MAS probes, ^{1}H{^{14}N} HMQC solid-state NMR experiments have become routine.[31–35] In the second approach, the transmitter offset of the pulses applied to the indirectly detected spin are incremented. The NMR spectrum of the indirectly detected spin is then reconstructed by plotting the response of the detected nucleus as a function of the pulse offset. This approach is especially useful for the quadrupolar nuclei because it can be applied even when the spectrum of the quadrupolar nucleus is megahertz broad, and it is not possible to coherently excite magnetization from the quadrupolar nucleus. These types of indirect detection experiments have been performed with pulse sequences such as Static Echo DOuble Resonance (SEDOR),[36–38] TRAnsfer of Population in DOuble Resonance (TRAPDOR),[39] Rotational Echo Adiabatic Passage DOuble Resonance (REAPDOR),[40,41] Resonance Echo Saturation Pulse DOuble Resonance (RESPDOR),[42–46] and PROgressive Saturation of the Proton Reservoir (PROSPR).[47,48] These experiments have been used to indirectly detect NMR spectra of quadrupolar nuclei such as ^{14}N, ^{27}Al, ^{17}O, ^{33}S and ^{35}Cl using ^{1}H or ^{13}C as the detected nucleus. We note that some of the examples cited above described acquisition of wideline solid-state NMR spectra of spin-1/2 nuclei broadened by chemical shift anisotropy (CSA).[36–38,46] Recently, we showed that CT wideline ^{35}Cl solid-state NMR spectra of partially Cl-terminated 2D silicon materials could be detected by plotting the dephasing observed in a ^{1}H{^{35}Cl} DE-RESPDOR experiments (Fig. 1B) as a function of the ^{35}Cl pulse offset.[42] Notably, for the 2D silicon materials, we were unable to observe a direct ^{35}Cl WURST-CPMG signal, presumably due to an unfavorable T_2' for the ^{35}Cl nuclei.[42]

Here we provide a detailed investigation of frequency-stepped RESPDOR experiments for the detection of wideline solid-state NMR spectra of I = 3/2 nuclei, using ^{35}Cl, ^{81}Br and ^{63}Cu as representative examples. We apply numerical SIMPSON simulations to investigate saturation pulse conditions that can be used to map out CT and ST wideline solid-state NMR spectra of I = 3/2 nuclei. We also simulate frequency-stepped dipolar dephasing experiments for higher spin quadrupolar nuclei.

Results and discussion

Pulse sequences used for direct detection and indirect detection solid-state NMR experiments

The most common pulse sequence used for direct detection of wideline solid-state NMR spectra of quadrupolar nuclei is WURST-CPMG (Fig. 1A).[19] We used WURST-CPMG to acquire ^{35}Cl and ^{81}Br solid-state NMR spectra of transplatin (*trans*-

 This journal is © the Owner Societies 2024

Open Access Article. Published on 16 January 2024. Downloaded on 2/10/2026 6:49:38 PM. This article is licensed under a Creative Commons Attribution-NonCommercial 3.0 Unported Licence.

$Cl_2Pt(NH_3)_2$), $MAPbCl_3$ ($(CH_3NH_3)PbCl_3$), and $MAPbBr_3$ ($(CH_3NH_3)PbBr_3$). Fig. 1B illustrates the $^1H\{X\}$ DE-RESPDOR pulse sequence.[49] DE-RESPDOR is preferred over a conventional RESPDOR experiment because it is more robust to experimental MAS frequency fluctuations.[49] We used DE-RESPDOR to perform ^1H detected ^{35}Cl and ^{81}Br solid-state NMR experiments. The Y{X}-heteronuclear spin echo (*J*-resolved) pulse sequence shown in Fig. 1C was used to indirectly detect ^{35}Cl and ^{63}Cu NMR spectra, using ^{207}Pb and ^{31}P as the spy nucleus, respectively. In both the DE-RESPDOR experiments and the *J*-resolved experiments, solid-state NMR spectra are reconstructed by plotting the dephasing as a function of the pulse offset as illustrated below.

Numerical simulations of dephasing in $^1H\{^{35}Cl\}$ DE-RESPDOR experiments

Prior to showing experimental NMR data, we have used SIMPSON[50–52] to simulate ^{35}Cl solid-state NMR spectra and illustrate how DE-RESPDOR can be used for indirect detection of ^{35}Cl. Fig. 2A shows the SIMPSON simulated static ^{35}Cl solid-state NMR spectra for transplatin with C_Q = 37.0 MHz, η_Q = 0.12 and an applied magnetic field of 9.4 T. Fig. 2B illustrates a spectrum simulated with the same parameters but with a magic angle spinning frequency of 50 kHz. In this case, the width of the central transition (CT) MAS powder pattern (*ca.* 5 MHz) greatly exceeds the MAS frequency (50 kHz), consequently, overlap of the CT MAS powder pattern with its spinning sideband powder patterns yields a spectrum that is nearly identical in appearance to a conventional static spectrum. Comparison of Fig. 2A and B suggests that MAS NMR experiments can provide the same spectrum and line shape as static NMR experiments, provided the width of the quadrupolar powder pattern greatly exceeds the MAS frequency.

Fig. 2C and D show SIMPSON simulated DE-RESPDOR dephasing heat maps. In the heat maps the offset of the saturation pulses

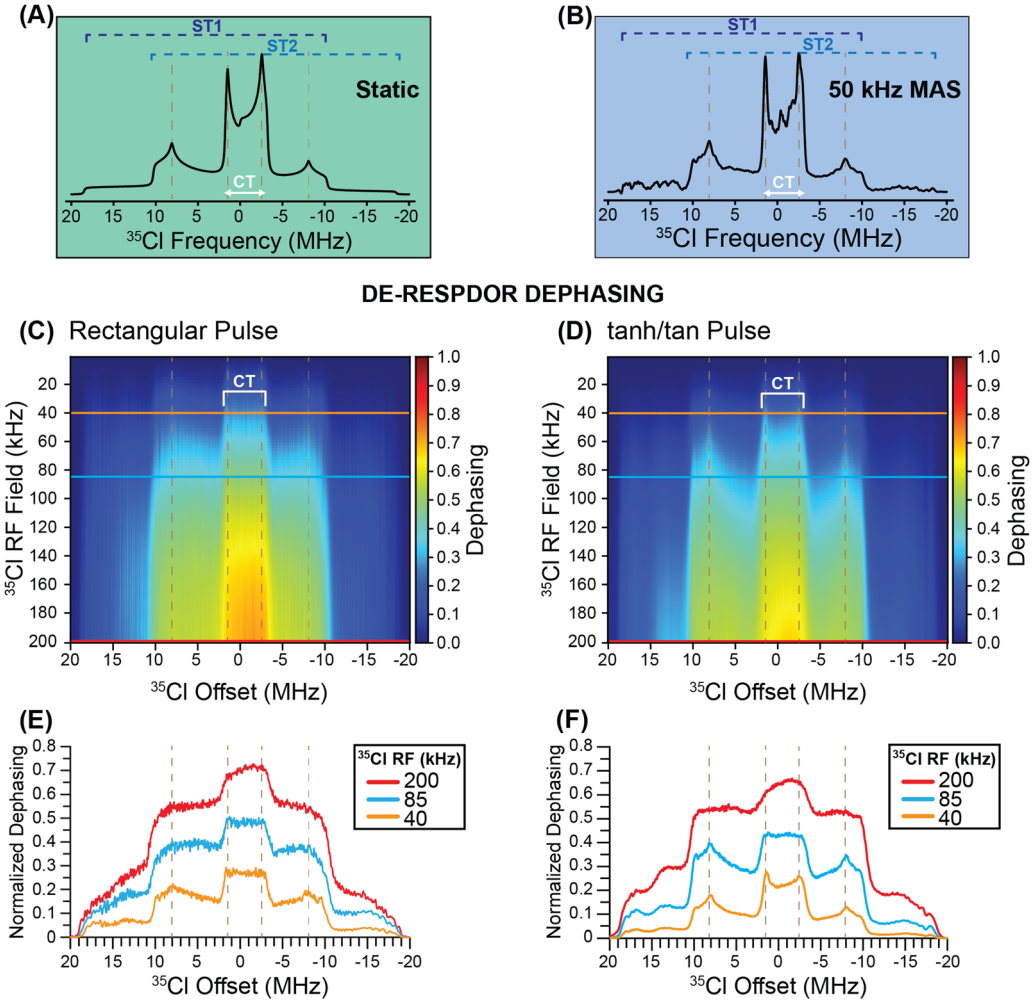

Fig. 2 SIMPSON simulated ^{35}Cl solid-state NMR spectra of transplatin (C_Q = 37 MHz and η_Q = 0.12) shown for (A) a static (stationary) sample and (B) for a 50 kHz magic angle spinning (MAS) frequency with a magnetic field of 9.4 T. (C) and (D) Heat plots showing the simulated dephasing for $^1H\{^{35}Cl\}$ DE-RESPDOR experiments as a function of the ^{35}Cl saturation pulse RF field and pulse offset. Simulations are shown for (C) conventional rectangular pulses 80 μs in duration and (D) frequency-swept tanh/tan pulses (ξ = 20, θ = 180°) using a frequency sweep of 5 MHz and 40 μs duration. All simulations used a $^1H-^{35}Cl$ spin system with a 2 kHz dipolar coupling constant. Dephasing profiles extracted from the heat plots for the ^{35}Cl saturation pulse RF fields 200 kHz, 85 kHz, and 40 kHz with (E) rectangular saturation pulses and (F) tanh/tan pulses.

Open Access Article. Published on 16 January 2024. Downloaded on 2/10/2026 6:49:38 PM.
This article is licensed under a Creative Commons Attribution-NonCommercial 3.0 Unported Licence.

is varied on the *x*-axis and the RF field of the saturation pulses is varied on the *y*-axis, while the color indicates the extent of dephasing. The dephasing is shown as a function of ^{35}Cl pulse power and offset with 80 μs (4 rotor cycles) rectangular pulses (Fig. 2C) and 40 μs frequency-swept tanh/tan pulses[53] with a 5 MHz sweep width (Fig. 2D). In Fig. 2E and F RESPDOR dephasing profiles are shown for ^{35}Cl saturation pulses with radiofrequency fields (RF) of 200, 85, and 40 kHz. The heatmaps and dephasing profiles illustrate that the plot of the dephasing as a function of the offset can roughly trace the CT and ST powder patterns. Because the CT is narrower than the ST, it is more easily saturated, resulting in enhanced dephasing in the RESPDOR experiments and a contrast between the CT and ST powder patterns. However, increasing the saturation pulse RF field increases the dephasing for both CT and ST, but also reduces the contrast between the CT and ST. The use of higher RF field saturation pulses also results in a rounding of the powder pattern discontinuities. It is well known in NMR experiments such as CEST,[54] that the saturation bandwidth will increase as the saturation pulse RF field is increased, resulting in broadening of the indirectly detected peaks. It is therefore unsurprising that the features in the dephasing profile become more rounded as the saturation pulses can create dephasing more effectively across the entire powder pattern when higher RF fields are used. Another interesting observation from Fig. 2 is that if shorter duration ^{35}Cl saturation pulses are used, then the discontinuities or "horns" associated with the ST are sharper than when rectangular pulses are applied. The tanh/tan pulses employed in Fig. 2D had a pulse length of 40 μs (two rotor cycles). Additional simulations with 40 μs rectangular saturation show similarly sharp features in the RESPDOR dephasing profile as were seen for the tanh/tan pulses (Fig. S3, ESI†). The 40 μs tanh/tan pulses use less RF power due to their hyperbolic tangent amplitude profile, and thus could be preferred experimentally.

In summary, it is evident from Fig. 2 that the RESPDOR dephasing profiles roughly map out the MAS solid-state NMR spectrum, including both the CT and ST regions of the powder pattern. Therefore, the simulations suggest that RESPDOR experiments can be used to indirectly detect wideline solid-state NMR spectra of spin 3/2 nuclei.

Experimental comparison of ^{1}H{^{35}Cl} DE-RESPDOR and direct WURST-CPMG for acquisition of the ^{35}Cl solid-state NMR spectrum of transplatin

Fig. 3A shows ^{1}H{^{35}Cl} DE-RESPDOR dephased spectrum (red, S) recorded with ^{35}Cl saturation pulses and the control spectrum (black, S_0) recorded without saturation pulses. All NMR spectra were acquired at B_0 = 9.4 T, with a ^{35}Cl saturation pulse that was four rotor cycles in duration (80 μs) with an 80 kHz RF field, and 3.84 ms of $SR4_1^2$ dipolar recoupling[55] applied to the ^{1}H spins. The NMR spectra shown in Fig. 3A were obtained with a ^{35}Cl pulse offset of 1.2 MHz. Control (S_0) and dephasing (S) ^{1}H NMR spectra show signal-to-noise ratios of 60 and 18 with eight scans, respectively. The difference spectrum (S_0-S, cyan) illustrated below has a signal-to-noise ratio of 30, which is adequate for indirect detection of ^{35}Cl in transplatin. We did not optimize the total recoupling time to obtain optimal sensitivity for the ^{1}H{^{35}Cl} DE-RESPDOR experiments for transplatin. Fig. S2 (ESI†) illustrates how to choose the optimal recoupling duration using ^{1}H{^{35}Cl} DE-RESPDOR experiments, using $MAPbCl_3$ as an example. In brief, the recoupling duration that maximizes the difference signal ($\Delta S = S_0 - S$) should be used. This optimal recoupling time can be found by making a plot of ΔS as a function of the recoupling duration (Fig. S2, ESI†).

^{1}H{^{35}Cl} DE-RESPDOR experiments on transplatin were performed where the offset of the ^{35}Cl saturation pulse was varied in steps of 400 kHz over a range of +3.4 to −4.6 MHz (Fig. 3B). For each ^{35}Cl pulse offset the probe needed to be manually retuned. Plotting the normalized signal dephasing ($\Delta S/S_0$) as a function of the ^{35}Cl saturation pulse offset enables the reconstruction of the MAS ^{35}Cl CT quadrupolar powder pattern for transplatin. Notably, the ^{1}H detected central transition ^{35}Cl solid-state NMR spectrum of transplatin was acquired in only *ca.* 27 minutes at B_0 = 9.4 T. Numerical simulations of the ^{1}H{^{35}Cl} DE-RESPDOR dephasing profile suggest that the ^{35}Cl C_Q is *ca.* 37 MHz (with η_Q = 0.1), in good agreement with ^{35}Cl C_Q value of 36.6 MHz previously reported by Lucier *et al.*[56] Note, that in order to fit the experimental RESPDOR saturation profile we must scale the simulated dephasing data. Scaling of the simulated dephasing is needed since we use two-spin simulations that assume 100% abundance of the quadrupolar nucleus and furthermore, the values of the ^{1}H–^{35}Cl dipolar coupling constants are unknown and challenging to measure. The variable offset cumulative spectrum (VOCS) ^{35}Cl WURST-CPMG spectrum of transplatin (black) was constructed by co-adding 21 individual sub-spectra (Fig. 3C). The analytically simulated (ssNake)[57] spectrum indicated the ^{35}Cl C_Q was 37 MHz with η_Q = 0.12. The co-added VOCS WURST-CPMG spectrum took 3 hours of spectrometer time to acquire (Fig. 3C).

The comparison of experimental time between indirectly detected ^{1}H{^{35}Cl} DE-RESPDOR experiments and directly detected ^{35}Cl WURST-CPMG experiments shows six-fold time-saving in indirect detection using ^{1}H as a spy nucleus. The signal-to-noise ratio was also 1.5 times higher in indirectly detected ^{35}Cl NMR spectra compared with the direct detection experiment. The gains in sensitivity obtained are even more impressive if one considers the amounts of sample used in the two types of experiments. ^{1}H{^{35}Cl} DE-RESPDOR experiments were performed with a 1.3 mm rotor that holds approximately 5 μL of sample, while the static ^{35}Cl WURST-CPMG experiments used *ca.* 100 μL of sample packed into a 4 mm rotor. Additionally, the ^{1}H T_1 determines the optimal recycle delay for the DE-RESPDOR experiments, while the ^{35}Cl T_1 determines the optimal recycle delay in the WURST-CPMG experiments. For transplatin we measured a ^{1}H T_1 of 17 s and used a recycle delay of 5 s for DE-RESPDOR experiments, while an experimentally optimized ^{35}Cl recycle delay of 0.5 s was used for ^{35}Cl WURST-CPMG experiments. Thus, samples with shorter and more favorable ^{1}H T_1 should show even higher gains in sensitivity for the indirect detection DE-RESPDOR NMR experiments.

One trade off with the wideline RESPDOR experiments is that the CT powder pattern discontinuities in the RESPDOR dephasing profiles are not as sharp as those seen in the direct

 This journal is © the Owner Societies 2024

Open Access Article. Published on 16 January 2024. Downloaded on 2/10/2026 6:49:38 PM.
This article is licensed under a Creative Commons Attribution-NonCommercial 3.0 Unported Licence.

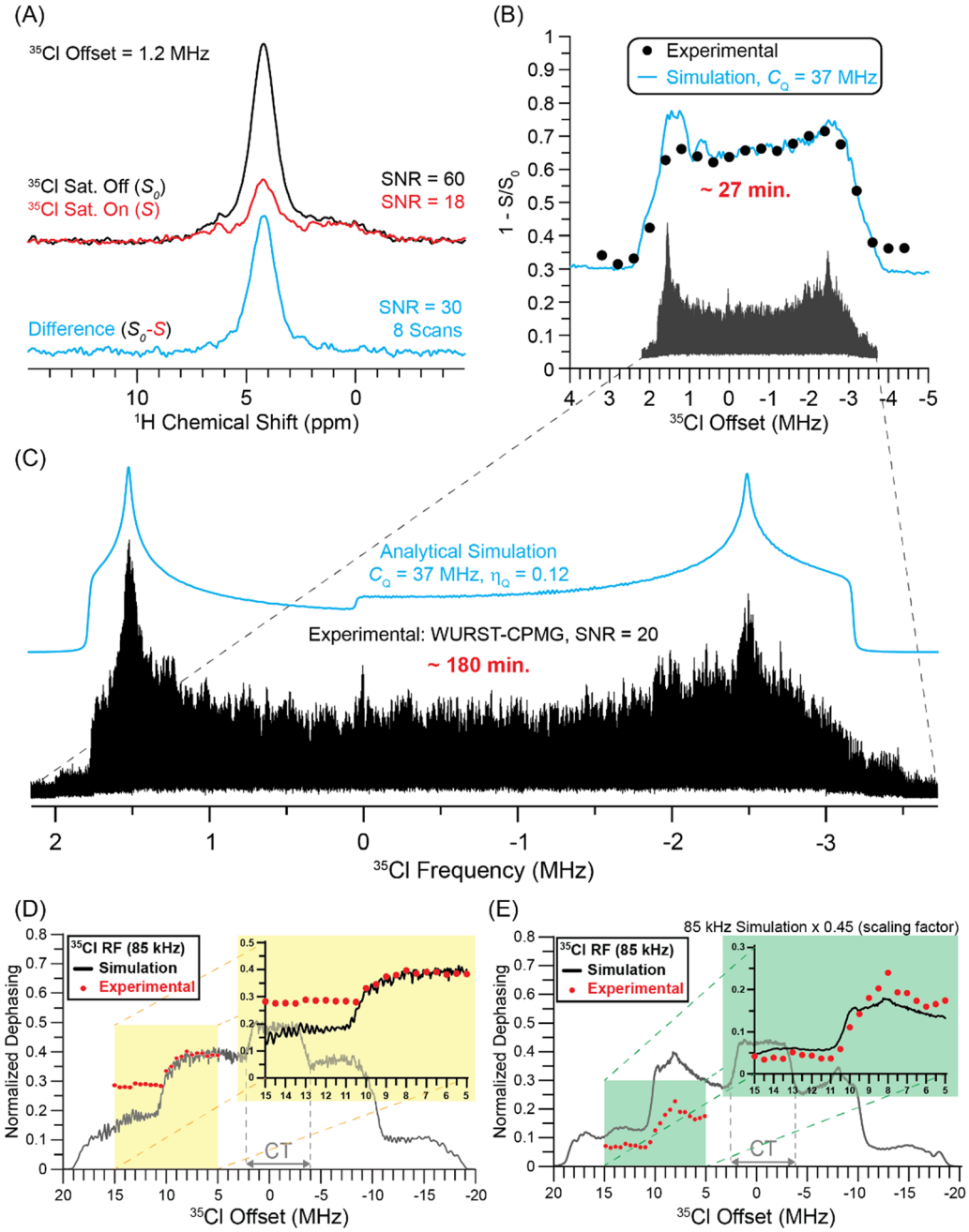

Fig. 3 Summary of ^{35}Cl solid-state NMR experiments on transplatin performed with a 9.4 T magnetic field. (A) 1D ^{1}H{^{35}Cl} DE-RESPDOR spectra recorded with (red) or without (black) 80 μs rectangular ^{35}Cl saturation pulses. The difference spectrum (cyan) is shown below. 8 scans were acquired for each spectrum, the MAS frequency was 50 kHz, and the total duration of $SR4_1^2$ dipolar recoupling was 3.84 ms. (B) Plot of ^{1}H{^{35}Cl} DE-RESPDOR normalized signal dephasing ($\Delta S/S_0$) as a function of the ^{35}Cl pulse offset over the CT region. The circles and lines correspond to experimental data points and numerical simulations, respectively. The same experimental parameters were used for the experiments shown in Fig. 3A and B. (C) VOCS WURST-CPMG static ^{35}Cl NMR spectrum of transplatin and simulation (cyan). Comparison of experimental and SIMPSON simulated ^{1}H{^{35}Cl} DE-RESPDOR dephasing for (D) rectangular ^{35}Cl saturation pulses 80 μs in duration and (E) tanh/tan pulses that are 40 μs in duration. The ^{35}Cl pulse offset was varied in steps of 500 kHz over the range of +5 MHz to +15 MHz.

acquisition WURST-CPMG NMR spectra, leading to reduced precision in the extraction of the C_Q and η_Q values. Fitting of the WURST-CPMG spectrum was reported to gives uncertainties of 0.1 to 0.3 MHz and 0.02 on the measured C_Q and η_Q values, respectively.[56] Simulations of the RESPDOR dephasing profiles with variable C_Q values suggest that the uncertainties on the measured values of C_Q are on the order of 1 MHz (Fig. S4, ESI†). The simulations suggest the η_Q value is between 0.0 and 0.25. Thus, there is likely a loss of precision in measurement of C_Q and η_Q as compared to direct detection methods. However, as is shown below, it is possible to improve the precision of the measured η_Q values by mapping out the ST powder patterns with RESPDOR experiments.

Open Access Article. Published on 16 January 2024. Downloaded on 2/10/2026 6:49:38 PM. This article is licensed under a Creative Commons Attribution-NonCommercial 3.0 Unported Licence.

Additional $^{1}H\{^{35}Cl\}$ DE-RESPDOR experiments on transplatin were performed where the offset of the ^{35}Cl saturation pulse varied in steps of 500 kHz over a range of +15 to +5 MHz in order to detect parts of the ^{35}Cl ST powder patterns. Corresponding SIMPSON simulated normalized dephasing profiles with 85 kHz RF field saturation pulses (black) are shown in Fig. 3D. Plotting the signal dephasing as a function of the ^{35}Cl saturation pulse offset enables the reconstruction of the partial MAS ST powder pattern for the transplatin. In Fig. 3D, there is a discrepancy between the experimental and simulated dephasing at different positions of the satellite transitions. The higher frequency part of the ST shows higher than expected dephasing. There are a number of reasons that explain this discrepancy. First, numerical simulations with a ^{1}H–^{35}Cl two-spin system show that the ratio of dephasing at the inner and outer part of the ST depends upon the recoupling duration (Fig. S5, ESI†). Second, the crystal structure of transplatin shows that each ^{1}H spin is coupled to several ^{35}Cl spins, meaning that a two-spin simulation is not an accurate representation of the experiments. Finally, the experimental ^{35}Cl RF field likely changes as the probe is retuned. While all of these factors could change the dephasing at different offsets, the most important constraint on the η_Q value is the position of the ''step'' arising from the overlap of the two satellite transitions.

Fig. 3E shows the simulated and experimental RESPDOR dephasing profiles obtained with ^{35}Cl tanh/tan saturation pulses with an 85 kHz RF field. The DE-RESPDOR experiments with the 40 μs tanh/tan pulses give well-defined ST discontinuities in both simulation and experiment, enabling η_Q to be more accurately determined. Fitting the ST region of the RESPDOR dephasing profile indicates that η_Q is between 0.0 and 0.1 (Fig. S3, ESI†). This is an important observation because the indirectly detected CT powder pattern is not very sensitive to η_Q. Therefore, if increased precision is required on measured values of η_Q then RESPDOR experiments can be performed to locate the ST discontinuities.

Comparison of direct detection and indirect detection for acquisition of the ^{35}Cl solid-state NMR spectrum of $MAPbCl_3$

Next, we investigated the use of indirect detection methods for acquisition of the ^{35}Cl solid-state NMR spectrum of methylammonium lead chloride ($MAPbCl_3$). Michaelis and co-workers have recently shown that ^{35}Cl solid-state NMR spectroscopy can be used to probe the structure of lead chloride perovskites and related phases.[58] The VOCS ^{35}Cl WURST-CPMG spectrum of $MAPbCl_3$ was obtained with 5 sub-spectra (Fig. 4A). Blue lines are numerically simulated spectra with a ^{35}Cl C_Q of 16.5 MHz (with $\eta_Q = 0$), which is consistent with the 16.34 MHz ^{35}Cl C_Q value reported by Sarkar *et al.*[58] The total experimental time to acquire the WURST-CPMG spectrum was 51 minutes, and the signal-to-noise ratio is approximately 160 at the most intense part of the CT powder pattern.

Fig. 4B depicts $^{1}H\{^{35}Cl\}$ DE-RESPDOR spectra with saturation pulses (red) and spectra without saturation pulses (black). With 16 scans, the control and dephasing spectra have signal-to-noise ratios of 150 and 52, respectively. The difference spectrum (cyan) shown below has a signal-to-noise ratio of 73. The spectra shown in Fig. 4B were obtained with a 0 MHz ^{35}Cl offset. All spectra were collected at B_0 = 9.4 T using a ^{35}Cl saturation pulse length of four rotor cycles (80 μs) with an 80 kHz RF field and 3.84 ms of $SR4_1^2$ dipolar recoupling.[55] Fig. S2 (ESI†) illustrates how to choose the optimal recoupling duration. Fig. S6 (ESI†) shows how varying the recoupling duration affects the quality of the indirectly detected ^{35}Cl NMR spectrum. The ^{35}Cl spectrum was indirectly detected with $^{1}H\{^{35}Cl\}$ DE-RESPDOR by varying the offset of the ^{35}Cl saturation pulse in 100 kHz steps over a range of +1.5 to −2 MHz (Fig. 4C). The ^{1}H detected ^{35}Cl NMR spectrum of $MAPbCl_3$ was obtained in *ca.* 25 minutes at B_0 = 9.4 T. However, as was seen above for transplatin, due to the RF field used for the ^{35}Cl saturation pulses, the CT pattern seen in the RESPDOR dephasing profile does not perfectly match the directly acquired CT powder pattern. Numerical simulations of the $^{1}H\{^{35}Cl\}$ DE-RESPDOR dephasing profile indicate that the ^{35}Cl C_Q is *ca.* 16.5 MHz (with $\eta_Q = 0$), consistent with the static WURST-CPMG spectrum. We note that the offset of the ^{35}Cl pulses was stepped in 100 kHz increments, resulting in lower resolution for the experimental RESPDOR dephasing profile as compared to the simulated one.

For $MAPbCl_3$ the sensitivity with ^{1}H detection is worse than the directly detected ^{35}Cl NMR spectrum. The gains in signal-to-noise ratio and time savings provided by ^{1}H detection is likely limited because the ^{1}H T_1 of $MAPbCl_3$ (T_1 = 30 s) is much longer than the ^{35}Cl T_1 (optimal recycle delays of 0.15 s). Furthermore, the ^{35}Cl homogeneous transverse relaxation time constant (T_2') is long enough to allow CPMG echoes to be acquired for *ca.* 50 ms, making CPMG detection efficient for $MAPbCl_3$. The relatively narrow breadth of the CT selective spectrum also means that only 5 WURST-CPMG sub-spectra need to be acquired. Thus, the results for $MAPbCl_3$ suggest that if the CT is less than 1 MHz in breadth and the ^{35}Cl T_2' is sufficiently long to allow efficient CPMG detection then direct detection is likely to be the preferred acquisition method. But we note that the $^{1}H\{^{35}Cl\}$ RESPDOR experiments may still be worthwhile since they provide valuable structural information by confirming that the ^{1}H spins of the MA cations are dipole coupled (spatially proximate) to the Cl anions.

We also attempted $^{207}Pb\{^{35}Cl\}$ *J*-resolved experiments to establish if ^{207}Pb could also be used as a spy nucleus for ^{35}Cl detection. Fig. 4D shows $^{207}Pb\{^{35}Cl\}$ *J*-resolved spectra recorded with (red) saturation pulses and without (black) saturation pulses. The pulse sequence for the *J*-resolved experiments is shown in Fig. 1C. The *J*-resolved experiments were performed at a field of 9.4 T with an MAS frequency of 25 kHz. The control and dephasing spectra have signal-to-noise ratios of 13 and 4, respectively. Each spectrum was obtained with 2048 scans and a 2 s recycle delay. The difference spectrum (cyan) shown below has an adequate signal-to-noise ratio of 5. The ^{35}Cl saturation pulse was two rotor periods in duration (80 μs) with a 41.7 kHz RF field, and the spin echo had a total duration of 0.64 ms. In this sample, the ^{207}Pb T_2' limits the echo duration and the achievable dephasing. $^{207}Pb\{^{35}Cl\}$ *J*-resolved experiments on $MAPbCl_3$ were performed with ^{35}Cl saturation pulse offsets varying in 200 kHz steps over a

 This journal is © the Owner Societies 2024

Open Access Article. Published on 16 January 2024. Downloaded on 2/10/2026 6:49:38 PM.
This article is licensed under a Creative Commons Attribution-NonCommercial 3.0 Unported Licence.

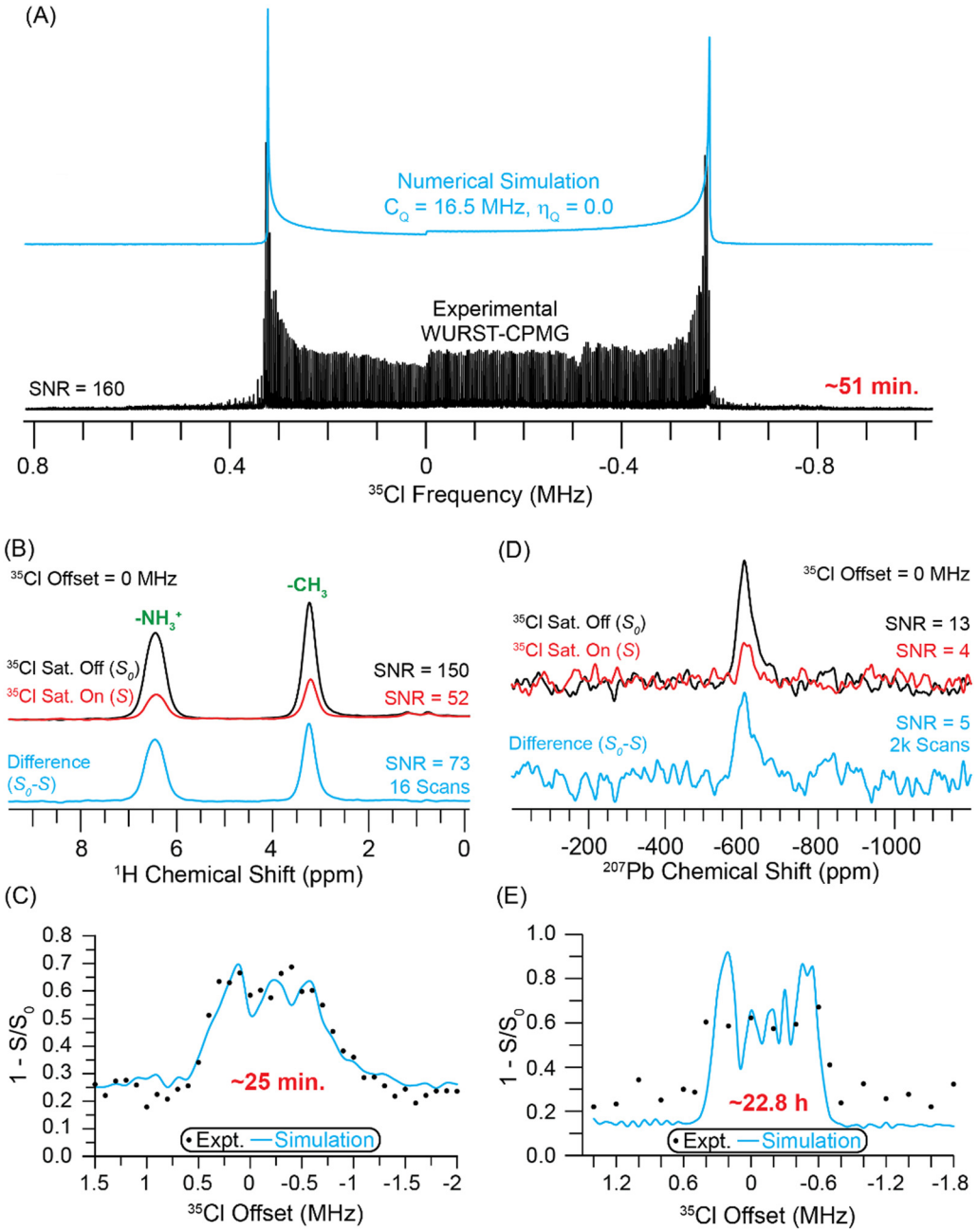

Fig. 4 (A) Static VOCS WURST-CPMG ^{35}Cl NMR spectrum of $MAPbCl_3$. (B) 1D ^{1}H{^{35}Cl} DE-RESPDOR spectra recorded with (red) or without (black) a ^{35}Cl saturation pulse and 3.84 ms of $SR4_1^2$ dipolar recoupling and a 50 kHz MAS frequency. A difference spectrum (cyan) is shown below. (C) Plot of ^{1}H{^{35}Cl} DE-RESPDOR signal dephasing as a function of the ^{35}Cl transmitter. (D) 1D ^{207}Pb{^{35}Cl} J-resolved spectra recorded (red) with or (black) without a ^{35}Cl saturation pulse and 0.64 ms of total J evolution time. (E) The plot of ^{207}Pb{^{35}Cl} J-resolved signal dephasing as a function of the ^{35}Cl transmitter recorded with a 25 kHz MAS frequency. In (C) and (E), the circles and lines correspond to experimental data points and numerical simulations, respectively. The simulation used a ^{35}Cl C_Q of 16.5 MHz. All experiments were performed with a magnetic field of 9.4 T.

range of +1.4 to −1.8 MHz. Plotting the signal dephasing as a function of the ^{35}Cl saturation pulse offset enables reconstruction of the MAS ^{35}Cl CT quadrupolar powder pattern for $MAPbCl_3$. The ^{207}Pb{^{35}Cl} J-resolved experiments required *ca.* 22.8 hours at B_0 = 9.4 T. In this case, ^{207}Pb detection would not be used to enhance the sensitivity of the ^{35}Cl NMR experiments, rather it would be used to obtain structural information because the ^{207}Pb{^{35}Cl} J-resolved experiments confirm that the lead atoms are covalently bound to chlorine atoms and that the C_Q of the chlorine atoms matches that observed in the directly acquired ^{35}Cl solid-state NMR spectrum.

^{1}H{^{81}Br} DE-RESPDOR and direct WURST-CPMG experiments on $MAPbBr_3$

We investigated the use of indirect detection methods for acquisition of the ^{81}Br solid-state NMR spectrum of methylammonium

Open Access Article. Published on 16 January 2024. Downloaded on 2/10/2026 6:49:38 PM.
This article is licensed under a Creative Commons Attribution-NonCommercial 3.0 Unported Licence.

lead bromide ($MAPbBr_3$). Previously, it was reported that the total ^{79}Br CT solid-state NMR spectrum of $MAPbBr_3$ required days of spectrometer time to acquire.[22] Due to the breadth of the ^{81}Br CT solid-state NMR spectrum (*ca.* 16 MHz), we only acquired a few VOCS sub-spectra close to the discontinuities of the ^{81}Br CT powder pattern (Fig. 5A). Blue lines are numerically simulated ^{81}Br solid-state NMR spectra with a ^{81}Br C_Q of 118 MHz (with η_Q = 0). The experimental time to acquire the two WURST-CPMG spectra was 41 minutes and the signal-to-noise ratio is approximately 117 at the most intense horn.

Fig. 5B depicts ^{1}H{^{81}Br} DE-RESPDOR spectra with (red) and without (black) ^{81}Br saturation pulses. All spectra were collected at B_0 = 14.1 T using a ^{81}Br saturation pulse length of four rotor cycles (80 μs) with a 50 kHz RF field and 1.92 ms of $SR4_1^{255}$ dipolar recoupling. With 8 scans, the control and dephasing spectra have signal-to-noise ratios of 420 and 340, respectively. The difference spectrum (cyan) shown below has a signal-to-noise ratio of 75. The spectra shown in Fig. 5B were obtained with a ^{81}Br pulse offset of −5 MHz. The ^{81}Br spectrum was then indirectly detected with ^{1}H{^{81}Br} DE-RESPDOR by varying the offset of the ^{81}Br saturation pulse in 1 MHz steps over a range of +10 to −14 MHz (Fig. 5C). The complete ^{1}H detected ^{81}Br solid-state NMR spectrum of $MAPbBr_3$ was obtained in *ca.* 64 minutes. Numerical simulations of the ^{1}H{^{81}Br} DE-RESPDOR dephasing profile indicate that the ^{81}Br C_Q is *ca.* 118 MHz (with η_Q = 0), consistent with the static VOCS WURST-CPMG spectrum. Note, a simulation of the ^{1}H{^{81}Br} DE-RESPDOR dephasing profile that also accounts for additional dephasing from ^{79}Br explains why the dephasing profile in Fig. 5C is asymmetric; at lower ^{81}Br transmitter offsets there is dephasing from the ^{79}Br ST (Fig. S7, ESI†).

Comparing the sensitivity of the indirectly detected ^{1}H{^{81}Br} DE-RESPDOR and the directly detected ^{81}Br WURST-CPMG reveals a slight sensitivity gain with ^{1}H detection. While the ^{81}Br WURST-CPMG spectrum of the high frequency horn has a signal-to-noise ratio of 117, this sub-spectrum required 20.5 minutes to acquire, corresponding to a sensitivity of 26 min$^{-1/2}$. In comparison, the ^{1}H{^{81}Br} DE-RESPDOR difference spectrum had a signal-

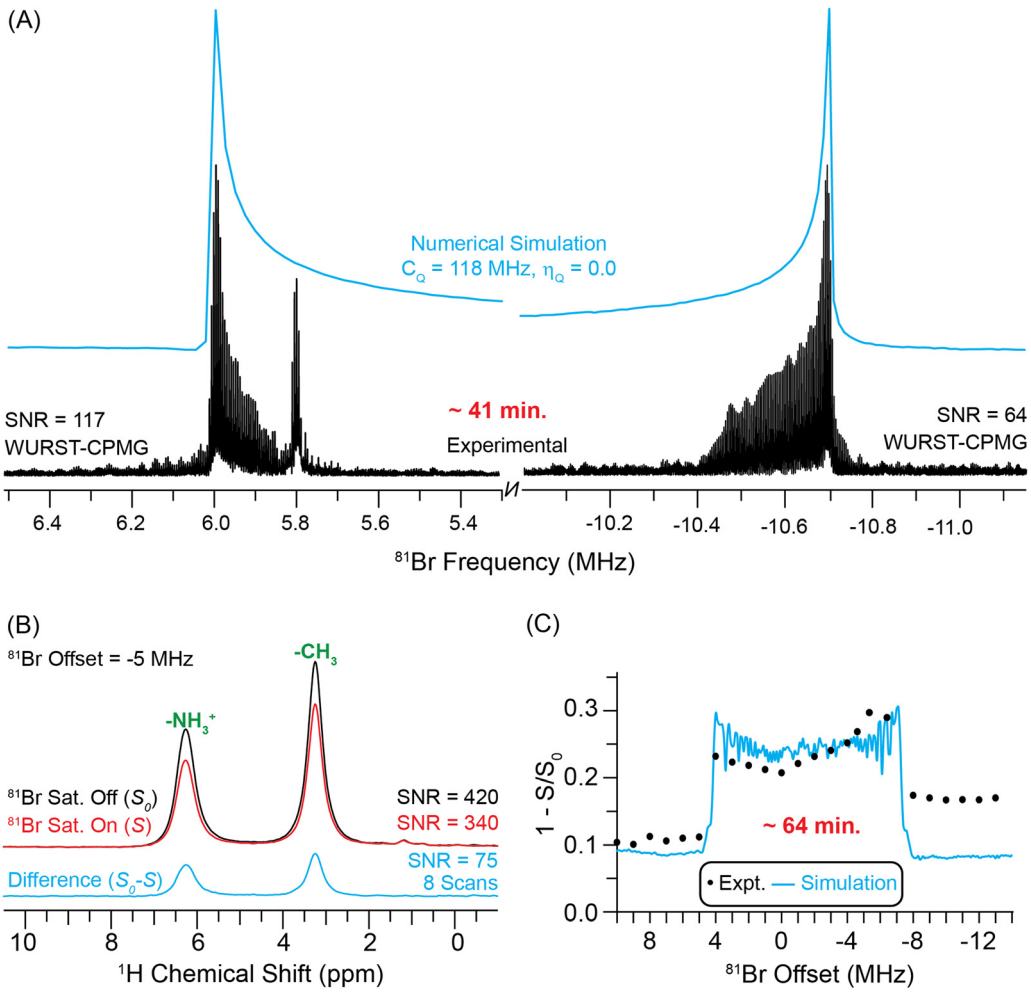

Fig. 5 (A) Static WURST-CPMG ^{81}Br NMR spectra of $MAPbBr_3$ obtained at a magnetic field of 9.4 T. (B) 1D ^{1}H{^{81}Br} DE-RESPDOR spectra recorded with (red) or without (black) a ^{81}Br saturation pulse, 1.92 ms of $SR4_1^2$ dipolar recoupling, a 25 kHz MAS frequency and a 14.1 T magnetic field. A difference spectrum (cyan) is shown below. (C) Plot of ^{1}H{^{81}Br} DE-RESPDOR dephasing as a function of the ^{81}Br transmitter offset. The circles and a line correspond to experimental data points and numerical simulations, respectively. The simulation used a ^{81}Br C_Q of 118 MHz.

 This journal is © the Owner Societies 2024

Open Access Article. Published on 16 January 2024. Downloaded on 2/10/2026 6:49:38 PM.
This article is licensed under a Creative Commons Attribution-NonCommercial 3.0 Unported Licence.

to-noise ratio of 75 in 3.2 minutes, corresponding to a sensitivity of 42 $min^{-1/2}$. Therefore, in this case the RESPDOR experiments provide a 1.6-fold improvement in sensitivity and 2.6-fold reduction in experiment time. For $MAPbBr_3$ the gain in signal-to-noise provided by ^1H detection is likely limited because the ^1H T_1 of $MAPbBr_3$ (T_1 = 24 s) is much longer than the ^{81}Br T_1 (optimal recycle delays of 0.12 s). However, we stress again that indirect detection also gives additional structural information by confirming that the ^1H spins of the MA^+ cations are dipole-coupled to the Br^- anions. We also note that the ^1H detected experiments required only a few μL of material, while we used 100 μL of material for the direct ^{81}Br WURST-CPMG experiments.

Indirect detection of the ^{63}Cu solid-state NMR spectrum of triphosCuI complex by $^1H \rightarrow {}^{31}P\{^{63}Cu\}$ J-resolved experiment

We studied the use of indirect detection methods for acquisition of the ^{63}Cu solid-state NMR spectrum of the copper(I) phosphine complex, $CH_3C(CH_2PPh_2)_3CuI$ (triphosCuI, Fig. S8, ESI†). Phosphines are common ligands coordinated to copper centers and phospine copper complexes are important catalysts, for example, for Sonogashira C–C cross-coupling reactions.[59] Therefore, it is interesting to determine whether ^{31}P-detection can be used as a method to obtain ^{63}Cu NMR spectra of copper complexes with phosphine ligands. The ^{63}Cu solid-state NMR signals of triphosCuI were narrow enough to obtain a CT MAS NMR spectrum that was free of spinning sidebands (Fig. 6A). Note, to acquire this spectrum we used the DEPTH pulse sequence[60] (with CT selective pulses) because the conventional spin echo NMR spectrum showed an intense ^{63}Cu NMR signal from copper metal components of the probe. A fit of the ^{63}Cu MAS NMR spectrum gave ^{63}Cu C_Q = 3.2 MHz, η_Q = 0.57 and δ_{iso} = 322 ppm. The total experimental time to acquire the DEPTH NMR spectrum was 205 minutes, and the signal-to-noise ratio was approximately 50. In this case, the ^{63}Cu NMR spectrum is quite narrow, and therefore, ^{31}P detection is not technically needed to study this compound. However, it is difficult to accurately determine the value of η_Q by only fitting the CT lineshape. Below, we show that indirect detections allow both the ^{63}Cu CT and ST powder patterns to be obtained and confirms the accuracy of the fitted value of η_Q.

Fig. 6B shows the MAS $^1H \rightarrow {}^{31}P\{^{63}Cu\}$ J-resolved NMR spectra obtained with (red) and without (black) a ^{63}Cu saturation pulse. The ^{31}P NMR spectrum shows two sets of NMR signals centered at −35 ppm and −43 ppm. Each set of signals in the ^{31}P NMR spectrum is composed of a 4-component multiplet that arises due to the combined effects of J-coupling and residual dipolar coupling to ^{63}Cu and ^{65}Cu nuclei that experience quadrupolar broadening (see a simulated spectrum in Fig. S10, ESI†). ^{31}P solid-state NMR spectra similar in appearance to the ones shown in Fig. 6B have been reported for other Cu(I) phosphine compounds.[61–63] The single crystal X-ray structure of triphosCuI shows that all three P atoms are crystallographically distinct (CCDC: 2250183†). The Cu–P bonds are similar in length for all P atoms (2.274 Å to 2.288 Å). However, two of the phosphorus atoms have similar I–Cu–P bond angles (126.1° and 123°), while the other I–Cu–P bond angle is 115.8°. Gauge-including

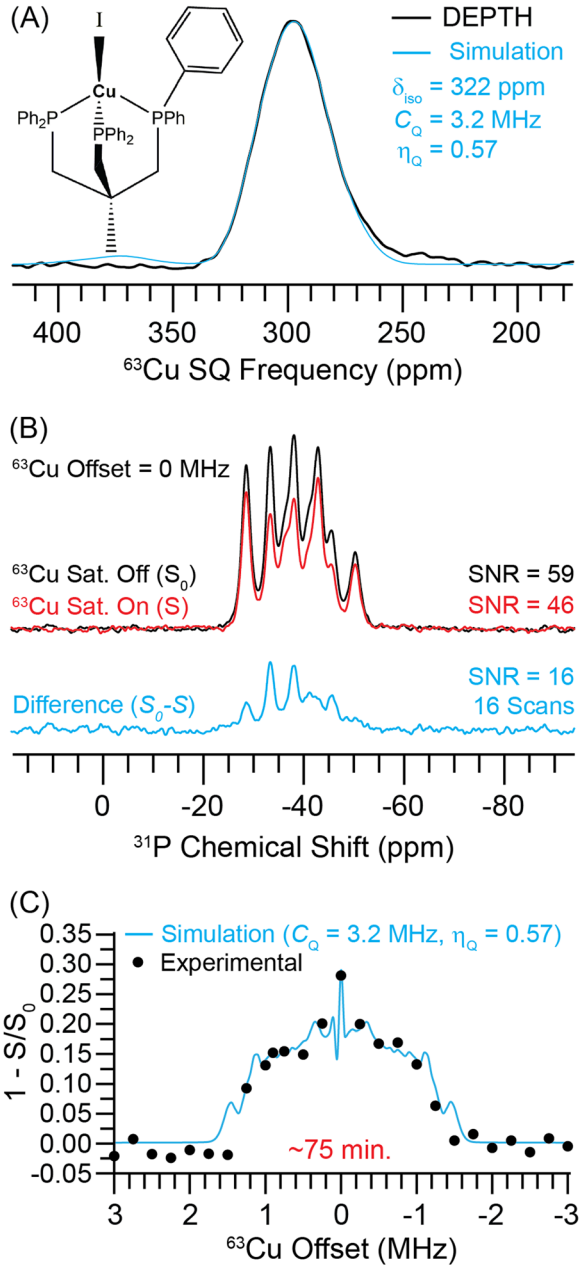

Fig. 6 (A) Experimental ^{63}Cu DEPTH NMR spectrum (black) and a simulation with a ^{63}Cu C_Q = 3.2 MHz and η_Q = 0.57 (cyan). (B) $^1H \rightarrow {}^{31}P\{^{63}Cu\}$ J-resolved NMR spectra recorded with (red) or without (black) a ^{63}Cu saturation pulse and 1.44 ms of total J evolution time. (C) $^1H \rightarrow {}^{31}P\{^{63}Cu\}$ J-resolved signal dephasing as a function of the ^{63}Cu transmitter recorded at B_0 = 9.4 T with 25 kHz MAS frequency. The circles and a line correspond to experimental data points and numerical simulation for a ^{63}Cu C_Q = 3.2 MHz and η_Q = 0.57 (cyan).

projector-augmented wave (GIPAW)[64] calculations implemented in the CASTEP[65] program was used to predict the ^{31}P magnetic shielding and differences in chemical shifts. The calculation predicts that two of the ^{31}P nuclei have similar magnetic shielding (σ_{iso} = 318.6 ppm and 320.5 ppm), while the third ^{31}P nucleus which has the I–Cu–P bond angle of 115.8° is approximately 15 ppm more shielded (σ_{iso} = 335.0 ppm). The predicted shieldings are in reasonable agreement with the

Open Access Article. Published on 16 January 2024. Downloaded on 2/10/2026 6:49:38 PM. This article is licensed under a Creative Commons Attribution-NonCommercial 3.0 Unported Licence.

experimental spectrum which shows higher intensity for the higher frequency ^{31}P NMR signals.

With 16 scans, the control and dephased ^{31}P NMR spectra have signal-to-noise ratios of 59 and 46, respectively. The difference spectrum (cyan) shown below has a signal-to-noise ratio of 16. The spectra shown in Fig. 6B were obtained with a 0 MHz ^{63}Cu offset. All spectra were collected at B_0 = 9.4 T using a ^{63}Cu saturation pulse length of one rotor cycle (40 s) and a total spin echo duration of 1.44 ms. The ^{63}Cu NMR spectrum was then indirectly detected with ^{1}H → ^{31}P{^{63}Cu} *J*-resolved experiments by varying the offset of the ^{63}Cu saturation pulse in 250 kHz steps over a range of +3 to −3 MHz (Fig. 6C). In Fig. 6C, we have integrated over all ^{31}P peaks. The ^{31}P detected ^{63}Cu NMR spectrum of triphosCuI was obtained in *ca.* 75 minutes at B_0 = 9.4 T. Numerical simulations of the ^{1}H → ^{31}P{^{63}Cu} *J*-resolved dephasing profile indicate that the ^{63}Cu C_Q is *ca.* 3.2 MHz (with η_Q = 0.57), in good agreement with the ^{63}Cu DEPTH NMR spectrum. Numerical simulations with different ^{63}Cu saturation pulse RF fields and different values of η_Q are shown in the ESI† (Fig. S9). With the current optimized saturation pulse condition of 30 kHz RF field, the dephasing profile remains sensitive to the value of η_Q.

Given the narrow width of the central transition ^{63}Cu NMR spectrum of triphosCuI, ^{31}P detection is not useful for sensitivity enhancement. However, the *J*-resolved experiments are still helpful in this case because they confirm the presence of coordinative bonds between the Cu and P atoms and confirms that the copper observed in the directly detected ^{63}Cu NMR spectrum gives rise to the observed dephasing.

Numerical simulations of dephasing in ^{1}H{^{35}Cl} DE-RESPDOR experiments as a function of ^{35}Cl C_Q

The dependence of the dephasing in a ^{1}H{^{35}Cl} DE-RESPDOR experiment on ^{35}Cl C_Q was investigated with numerical SIMPSON simulations. Fig. 7 shows normalized dephasing as a function of ^{35}Cl C_Q for a 50 kHz MAS frequency with a magnetic field of 9.4 T for 200 kHz, 80 kHz, and 40 kHz saturation pulse RF fields. The ^{35}Cl saturation pulse was 80 μs in duration. Each curve was constructed by varying C_Q from 1 to 80 MHz with 1 MHz increments while maintaining η_Q constant at 0.5 and considering the dephasing at ^{35}Cl transmitter offset = 0 MHz for each data point. The dephasing is significantly higher at 200 kHz RF field for the ^{35}Cl C_Q range considered in this simulation. However, such a high ^{35}Cl RF field may not be possible to achieve experimentally. For the other two saturation pulse RF fields of 80 kHz and 40 kHz, the dephasing gradually decreases as the ^{35}Cl C_Q increases. But, even if the ^{35}Cl pulse RF field was limited to 40 kHz appreciable dephasing is still predicted. Notably, Cl covalently bonded to Cl has a C_Q on the order of 75 MHz.[66] Therefore, the ^{1}H{^{35}Cl} DE-RESPDOR experiments could even be applicable to detection of covalently bonded chlorine atoms in organic systems.

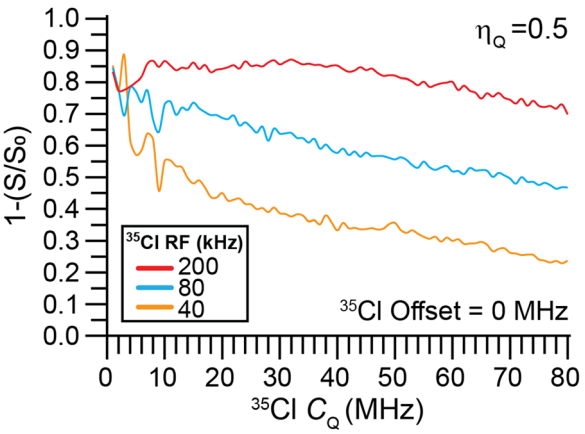

Fig. 7 SIMPSON simulated dependence of the normalized ^{1}H{^{35}Cl} DE-RESPDOR dephasing ($1 - S/S_0$) on the ^{35}Cl C_Q. Simulations were performed with a 50 kHz magic angle spinning (MAS) frequency with a magnetic field of 9.4 T. Simulations used 80 μs ^{35}Cl saturation pulses with RF fields of 200 kHz, 80 kHz, or 40 kHz. All simulations used a ^{1}H–^{35}Cl spin system with a 2 kHz dipolar coupling constant and η_Q = 0.5.

Numerical simulations of RESPDOR experiments with I = 5/2 and 7/2 nuclei

One obvious question that arises from the previous results is whether or not the indirect detection methods can potentially be applied to quadrupolar nuclei with spins greater than 3/2. To address this question, we have performed SIMPSON simulations of DE RESPDOR experiments for representative 5/2 (^{127}I, Fig. 8) and 7/2 nuclei (^{51}V, Fig. 8). Fig. 8 shows SIMPSON simulated ^{127}I and ^{51}V NMR spectra and DE RESPDOR dephasing plots for the two test cases of $BaI_2{\cdot}2H_2O$[26] and $V_2O_2(OH)_3$,[67] respectively. The ^{127}I C_Q and η_Q of $BaI_2{\cdot}2H_2O$ has been previously measured, while the C_Q and η_Q of $V_2O_2(OH)_3$ were obtained from a plane-wave DFT calculation. The SIMPSON simulations clearly suggest that the frequency stepped RESPDOR experiments should be applicable to higher spin nuclei. However, we note that it is possibly more challenging to resolve the CT from the ST since there are more ST for higher spin quadrupolar nuclei. Additionally, there may be significant broadening of the powder patterns, especially if higher RF fields are used for the saturation pulses. For example, in the simulated ^{1}H{^{51}V} RESPDOR dephasing profiles the powder pattern is significantly broadened due to off-resonance saturation effects. We plan to experimentally test these approaches for I = 5/2 and I = 7/2 nuclei in future work.

3. Conclusions

In conclusion, we have demonstrated that frequency-stepped dephasing experiments can be used for the indirect detection of wideline solid-state NMR spectra of abundant spin-3/2 nuclei. For the test cases considered in this paper, significant time savings and gains in sensitivity were realized in some cases. The exact gains in sensitivity that are achievable with indirect detection depend upon the ratio of the ^{1}H T_1 and quadrupolar nucleus T_1 and the spin quantum number and γ of the quadrupolar nucleus. Additional factors that influence the gains in sensitivity include the magnitude of the dipolar or scalar couplings and T_2' of the quadrupolar nucleus, with the latter

 This journal is © the Owner Societies 2024

Open Access Article. Published on 16 January 2024. Downloaded on 2/10/2026 6:49:38 PM.
This article is licensed under a Creative Commons Attribution-NonCommercial 3.0 Unported Licence.

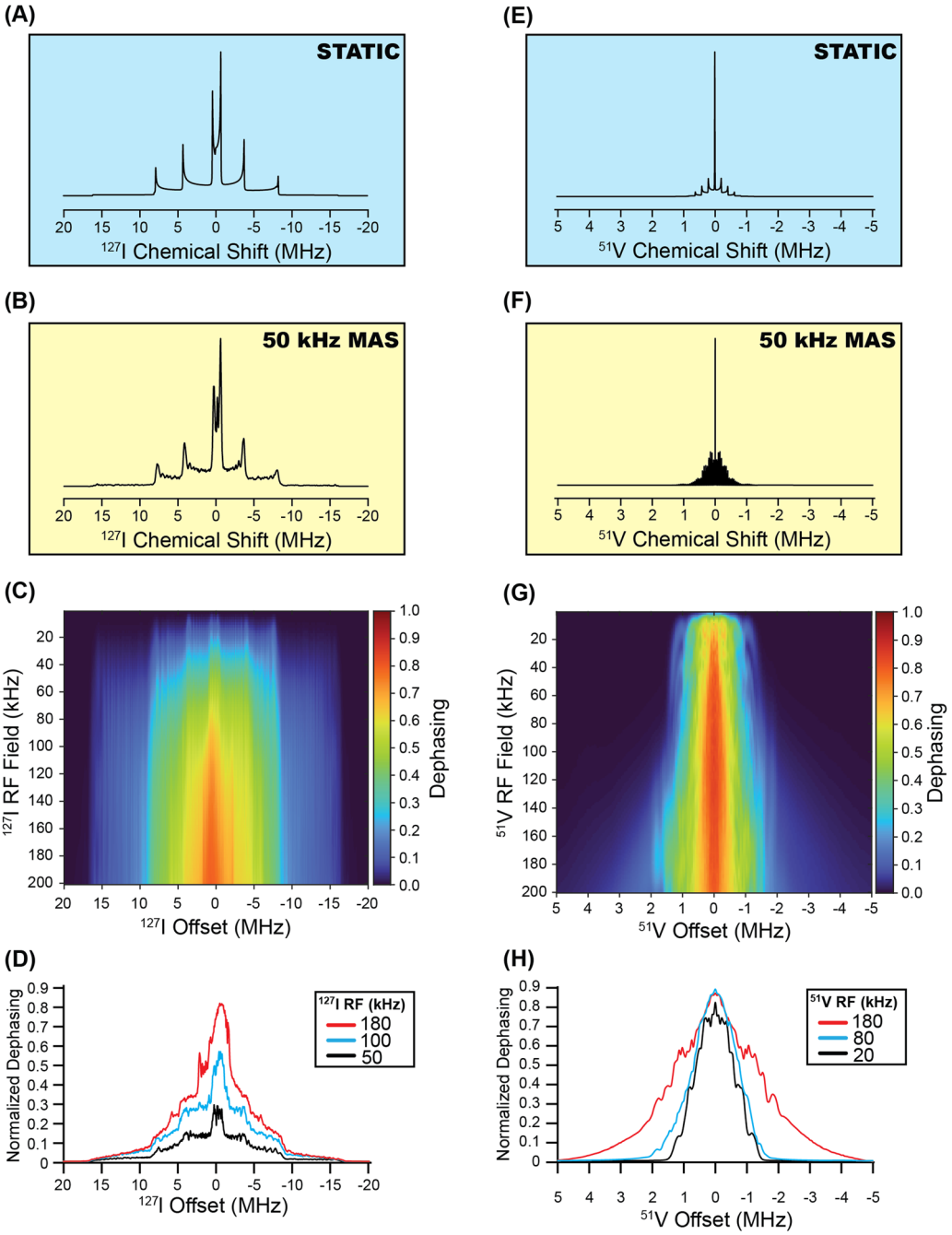

Fig. 8 SIMPSON simulated ^{127}I solid-state NMR spectra of $BaI_2{\cdot}2H_2O$ (C_Q = 53.8 MHz and η_Q = 0) shown for (A) a stationary sample and (B) for a 50 kHz MAS frequency. (C) Heat plot showing the simulated dephasing for ^{1}H{^{127}I} DE-RESPDOR experiments as a function of the ^{127}I saturation pulse RF field with conventional rectangular pulses that are 80 μs in duration. (D) Dephasing profiles extracted from the heat plot for ^{127}I saturation pulse RF fields of 180 kHz, 100 kHz, and 50 kHz. SIMPSON simulated ^{51}V solid-state NMR spectra of $V_2O_2(OH)_3$ (C_Q = 5.8 MHz and η_Q = 0.33) shown for (E) a stationary sample and (F) for a 50 kHz MAS frequency. (G) Heat plot showing the simulated dephasing for ^{1}H{^{51}V} DE-RESPDOR experiments as a function of the ^{51}V saturation pulse RF field with conventional rectangular pulses that are 80 μs in duration. (H) Dephasing profiles extracted from the heat plot for ^{51}V saturation pulse RF fields 180 kHz, 80 kHz, and 20 kHz.

parameter determining how efficient CPMG detection can be. The breadth of the quadrupolar powder pattern is also an important consideration, with indirect detection likely preferred for wider spectra and direct detection preferred for narrower quadrupolar powder patterns. Even in cases where the indirect detection dephasing experiments do not provide absolute gains in sensitivity, they may still be helpful as they provide valuable structural information by confirming the presence of dipolar or scalar couplings between the detected nucleus and the quadrupolar nucleus of interest. We also note that much smaller sample volumes are required for the indirect detection experiments, so they should be useful for limited

Open Access Article. Published on 16 January 2024. Downloaded on 2/10/2026 6:49:38 PM. This article is licensed under a Creative Commons Attribution-NonCommercial 3.0 Unported Licence.

quantity samples. Numerical simulations suggest that the RESPDOR methods are applicable to samples with very large C_Q.

We anticipate that the indirect detection experiments demonstrated here can be readily combined with dynamic nuclear polarization (DNP) to further enhance sensitivity.[68] Under MAS conditions DNP-enhanced ^{1}H spin polarization can be efficiently transferred to spin-1/2 nuclei such as ^{1}H, ^{13}C and ^{31}P, whereas direct DNP or indirect DNP of quadrupolar nuclei is often more challenging. Hence, the indirect detection approach is potentially easier to implement in DNP experiments. We are pursuing further research along these lines. Another interesting direction to consider would be to incorporate phase-modulated (PM) saturation pulses[69,70] into the DE-RESPDOR experiments. The PM saturation pulses have been shown to provide enhanced dephasing in REDOR experiments with quadrupolar nuclei that exhibit large quadrupolar coupling constants.[69,70] For samples with very large C_Q, the PM pulses may be beneficial. We are actively using these indirect detection methods to study materials that contain quadrupolar nuclei that give rise to wideline solid-state NMR spectra.

4. Experimental

Transplatin was purchased from Alfa Aesar and used without further purification. Methylammonium bromide (CH_3NH_3Br) was purchased from DyeSol. Methylammonium chloride (CH_3NH_3Cl, 99.0%) and lead chloride ($PbCl_2$, 99.999%) were purchased from Sigma-Aldrich. Lead bromide ($PbBr_2$, 98 + %) was purchased from Acros. *N*,*N*-Dimethylformamide (DMF) and toluene were purchased from Fisher Scientific. Copper(I) iodide (CuI, 95 + %) was purchased from Alfa Aesar and used after purification. 1,1,1-Tris(diphenylphosphinomethyl)ethane (triphos, 97 + %) was purchased from Strem. Chloroform was purchased from BeanTown Chemical and used after vacuum distillation over sieves. $MAPbCl_3$, $MAPbBr_3$ and triphosCuI were prepared according to the following procedures:

Synthesis of methylammonium lead halides

$CH_3NH_3PbBr_3$ and $CH_3NH_3PbCl_3$ were synthesized by a slightly modified literature procedure.[71,72] Briefly, CH_3NH_3Br (1.5 mmol) and $PbBr_2$ (1.5 mmol) were dissolved in DMF (30 mL). After stirring until the mixture became homogeneous (<30 min), excess toluene (100 mL) was added. Crystalline $CH_3NH_3PbBr_3$ was collected by centrifugation at 4000 rpm for 10 min. After washing 3 times with toluene (30 mL), the material was dried under vacuum. $CH_3NH_3PbCl_3$ was synthesized from CH_3NH_3Cl and $PbCl_2$ following a similar procedure. Synthesis of $CH_3NH_3PbBr_3$ and $CH_3NH_3PbCl_3$ was confirmed by powder X-ray diffraction (PXRD, Fig. S11, ESI†). PXRD patterns were recorded using Cu Kα radiation on a Rigaku Ultima IV diffractometer (40 kV, 44 mA).

Synthesis of the complex triphosCuI

A flask was charged with 1,1,1-tris(diphenylphosphinomethyl)ethane (111.3 mg, 0.1782 mmol), CuI (32.5 mg, 0.171 mmol), and 25 mL of chloroform under nitrogen. The reaction mixture was stirred overnight, forming a crystalline precipitate. The mixture was filtered, and the solids were washed with 3 mL of chloroform, then dried *in vacuo*. A colorless powder (103.5 mg, 0.1270 mmol, 71.3%) was collected. Solution ^{1}H NMR spectra and single crystal X-ray diffraction data are included in the ESI.† The single-crystal X-ray diffraction structure of triphosCuI can be accessed from the Cambridge Crystallographic Data Centre (CCDC code: 2250183).

Solid-state NMR spectroscopy

Solid-state NMR spectroscopy experiments were performed on a 9.4 T Bruker wide-bore magnet equipped with a Bruker AVANCE III HD console (^{1}H{^{35}Cl} DE-RESPDOR,[49] ^{35}Cl and ^{81}Br WURST-CPMG,[19] ^{207}Pb{^{35}Cl} *J*-resolved, ^{63}Cu DEPTH[60] and ^{1}H → ^{31}P{^{63}Cu} *J*-resolved) and equipped with a Bruker 1.3 mm HX (^{1}H{^{35}Cl} experiments of transplatin and $MAPbCl_3$), Bruker 2.5 mm HXY probe (^{207}Pb{^{35}Cl} of $MAPbCl_3$ and ^{1}H → ^{31}P{^{63}Cu} of triphosCuI complex) or a Bruker 4.0 mm HXY magic angle spinning (MAS) NMR probe (all WURST-CPMG experiments). ^{1}H{^{81}Br} experiments were performed with a 14.1 T Bruker wide-bore magnet equipped with a Bruker AVANCE NEO console and a Bruker 2.5 mm HXY MAS NMR probe. All experiments utilized N_2 gas for spinning. ^{1}H chemical shifts were referenced to neat tetramethylsilane by using adamantane ($\delta_{iso}(^1H)$ = 1.72 ppm) as a secondary chemical shift reference. ^{207}Pb and ^{31}P chemical shifts were indirectly referenced to neat TMS using the IUPAC recommended relative NMR frequency.[73] NMR spectra were processed and analyzed with Bruker Topspin version 3.6.4 (AVANCE III HD data) or 4.1.4 (AVANCE NEO data) software.

The following experimental details are with respect to data acquired at B_0 = 9.4 T with the 1.3 mm HX NMR probe (^{1}H{^{35}Cl} experiments), 2.5 mm HXY NMR probe (^{207}Pb{^{35}Cl} and ^{1}H → ^{31}P{^{63}Cu} experiments) and 4 mm HXY NMR probe (WURST-QCPMG experiments). ^{1}H{^{35}Cl} DE-RESPDOR spectra of transplatin were recorded with the 1.3 mm HX NMR probe and a 50 kHz MAS frequency. The ^{1}H longitudinal relaxation time constant (T_1) of transplatin was *ca.*17 s; all experiments utilized a 5 s recycle delay. ^{1}H{^{35}Cl} DE-RESPDOR experiments were performed with ^{35}Cl saturation pulses that were 80 μs ($4 \times \tau_{rot}$) in duration with an 80 kHz RF field.[49] Additional experiments on transplatin were performed with tanh/tan ^{35}Cl saturation pulses 40 μs in duration. The sweep width of the tanh/tan pulses was set to 5 MHz. The $SR4_1^2$ heteronuclear dipolar recoupling sequence was applied to the ^{1}H spins to reintroduce the ^{1}H–^{35}Cl dipolar interaction under MAS.[55] A control (without a ^{35}Cl saturation pulse) and dephased (with a ^{35}Cl saturation pulse) point were recorded at each ^{35}Cl offset. Similarly, ^{1}H{^{35}Cl} DE-RESPDOR spectra of $MAPbCl_3$ were recorded with the 1.3 mm HX NMR probe and a 50 kHz MAS frequency. The ^{1}H T_1 of $MAPbCl_3$ was *ca.* 24 s and 30 s for high-frequency (NH_3^+) and low-frequency ^{1}H NMR signal ($-CH_3$), respectively; all experiments utilized a 5 s recycle delay and the high-frequency ^{1}H NMR signal was used to map out the ^{35}Cl spectrum. ^{1}H{^{35}Cl} DE-RESPDOR experiments were performed with ^{35}Cl saturation

 This journal is © the Owner Societies 2024

Open Access Article. Published on 16 January 2024. Downloaded on 2/10/2026 6:49:38 PM. This article is licensed under a Creative Commons Attribution-NonCommercial 3.0 Unported Licence.

pulses that were 80 μs ($4 \times \tau_{rot}$) in duration with an 80 kHz radio frequency (RF) field.[49] The $SR4_1^2$ heteronuclear dipolar recoupling sequence was applied to the ^{1}H spins to reintroduce the ^{1}H–^{35}Cl dipolar interaction under MAS.[55] A control (without a ^{35}Cl saturation pulse) and dephased (with a ^{35}Cl saturation pulse) point was recorded at each ^{35}Cl offset. ^{207}Pb{^{35}Cl} *J*-resolved spectra of $MAPbCl_3$ were recorded with the 2.5 mm HXY NMR probe and a 25 kHz MAS frequency. All experiments utilized a 2 s recycle delay. ^{207}Pb{^{35}Cl} *J*-resolved experiments were performed with ^{35}Cl saturation pulses that were 80 μs ($2 \times \tau_{rot}$) in duration with a 14 kHz RF field. A control (without a ^{35}Cl saturation pulse) and dephased (with a ^{35}Cl saturation pulse) point were recorded at each ^{35}Cl offset. ^{1}H → ^{31}P{^{63}Cu} *J*-resolved spectra of triphosCuI were recorded with the 2.5 mm HXY NMR probe and a 25 kHz MAS frequency. The ^{1}H T_1 of triphosCuI complex was *ca.* 6.4 s; all experiments utilized an 8 s recycle delay. ^{1}H → ^{31}P{^{63}Cu} *J*-resolved experiments were performed with ^{63}Cu saturation pulses that were 40 μs ($1 \times \tau_{rot}$) in duration with a 30 kHz RF field. A control (without a ^{63}Cu saturation pulse) and dephased (with a ^{63}Cu saturation pulse) point were recorded at each ^{63}Cu offset. The ^{63}Cu DEPTH[60] spectrum was recorded with 3 s recycle delay and 4096 scans. Static WURST-QCPMG spectra of $MAPbCl_3$ were recorded with the 4 mm HXY NMR probe with WURST pulses that were 25 μs in duration and with a sweep width of 800 kHz.[19,24,74] Each echo in the CPMG train was 50 μs in duration. A total of 30 echoes were acquired. 50 kHz ^{1}H RF field SPINAL-64 decoupling was performed throughout the entire static CPMG experiments.[75] Similarly, static WURST-QCPMG spectra of transplatin were recorded with the 4 mm HXY NMR probe with WURST pulses that were 50 μs in duration and with a sweep width of 800 kHz.[19,24,74] Each echo in the CPMG train was 90 μs in duration. A total of 100 echoes were acquired. High-frequency and low-frequency ends were recorded for static WURST-QCPMG spectra of $MAPbBr_3$ with the 4 mm HXY NMR probe with WURST pulses that were 25 μs in duration and with a sweep width of 800 kHz.[19,24,74] Each echo in the CPMG train was 50 μs in duration. A total of 10 echoes were acquired.

The following experimental details are for data collected with the Bruker 2.5 mm HXY NMR probe and B_0 = 14.1 T (^{1}H{^{81}Br} experiments). ^{1}H{^{81}Br} DE-RESPDOR spectra of $MAPbBr_3$ were recorded with a 25 kHz MAS frequency. The ^{1}H T_1 of $MAPbBr_3$ was *ca.* 24 s and 23 s for high-frequency ($-NH_3^+$) and low-frequency signal ($-CH_3$), respectively. All experiments applied a 10 s recycle delay and considered high-frequency signal to map out the ^{81}Br spectrum. ^{1}H{^{81}Br} DE-RESPDOR experiments were performed with ^{81}Br saturation pulses that were 80 μs ($2 \times \tau_{rot}$) in duration with a 50 kHz RF field.[49] The $SR4_1^2$ heteronuclear dipolar recoupling sequence was applied to the ^{1}H spins to reintroduce the ^{1}H–^{81}Br dipolar interaction under MAS.[55] A control (without a ^{81}Br saturation pulse) and dephased (with a ^{81}Br saturation pulse) point was recorded at each ^{81}Br offset.

Numerical solid-state NMR spectroscopy simulations

SIMPSON v4.1.1 was used to perform numerical solid-state NMR simulations.[50–52] The archived data includes the SIMPSON input codes. Except for the ^{1}H $\pi/2$ pulses, all the pulses in the files were finite in duration. All 2D heat maps were created using the rep678 crystal file. Static and MAS ideal ^{35}Cl NMR spectra were simulated using the zcw28656 crystal file. The number of gamma angles was 15 for the MAS spectrum simulations. In Fig. 2C and D, the ^{35}Cl offset was incremented in steps of 50 kHz over a frequency range of +20 MHz to −20 MHz while the ^{35}Cl saturation RF field was increased in steps of 2 kHz from 0 to 200 kHz. The simulations in Fig. 2E were extracted from the simulation corresponding to Fig. 2C. The simulation in Fig. 2F was extracted from corresponding simulations shown in Fig. 2D. MATLAB R2021B was used to create all heat maps. The simulated spectra were processed in ssNake v1.3.[57] The DE-RESPDOR heat maps were normalized by dividing each dephasing intensity by the maximum dephasing exhibited in each heat map. All the other numerical simulations were run with identical parameters (RF fields, transmitter offsets, and B_0) to those used experimentally. The other numerical simulations for ^{1}H{^{35}Cl} DE-RESPDOR in Fig. 2B and 4C were performed with a two-spin ^{1}H–^{35}Cl spin system, the zcw4180 crystal file, 13 γ-angles, and a 0.5 μs time step where the Hamiltonian was considered time-independent. ^{1}H{^{81}Br} DE-RESPDOR numerical simulations were done with a two-spin ^{1}H–^{81}Br spin system, the zcw4180 crystal file, 13 γ-angles, and a 0.1 μs time step where the Hamiltonian was considered time-independent. Numerical simulations of static ^{35}Cl/^{81}Br solid-state NMR spectra were performed with the zcw28656 crystal file and assumed ideal excitation of the powder pattern (start operator I_{1x}, detect operator I_{1c}). In Fig. 8, all 2D heat maps were created using the rep678 crystal file. Static and MAS ideal ^{35}Cl NMR spectra were simulated using the zcw28656 crystal file. The number of gamma angles was 15 for the MAS spectrum simulations. In Fig. 8C, the ^{127}I offset was incremented in steps of 50 kHz over a frequency range of +20 MHz to −20 MHz while the ^{127}I saturation RF field was increased in steps of 2 kHz from 0 to 200 kHz. The simulation in Fig. 8D was extracted from the simulation corresponding to Fig. 8C.

In Fig. 8G, the ^{51}V offset was incremented in steps of 50 kHz over a frequency range of +5 MHz to −5 MHz while the ^{51}V saturation RF field was increased in steps of 1 kHz from 0 to 200 kHz. The simulation in Fig. 8H was extracted from the simulation corresponding to Fig. 8G. MATLAB R2021B was used to create all heat maps. The simulated spectra were processed in ssNake v1.3.[57]

Conflicts of interest

There are no conflicts of interest to declare.

Acknowledgements

Material synthesis, solid-state NMR experiments and simulations were supported by the US Department of Energy (DOE), Office of Science, Basic Energy Sciences, Materials Science and Engineering Division (A. J. R., J. V., S. N. S. L, B. A. A., R. W. D., and E. G.). The Ames Laboratory is operated for the US DOE by

Open Access Article. Published on 16 January 2024. Downloaded on 2/10/2026 6:49:38 PM. This article is licensed under a Creative Commons Attribution-NonCommercial 3.0 Unported Licence.

Iowa State University under Contract DE-AC02-07CH11358. Synthesis, characterization and NMR experiments on triphosCuI were supported by grant CHE-1900100 from the US NSF (J. B. and M. R. K). A. J. R. acknowledges additional support from the Alfred P. Sloan Foundation through a Sloan research fellowship.

References

1 S. P. Brown and H. W. Spiess, Advanced solid-state NMR methods for the elucidation of structure and dynamics of molecular, macromolecular, and supramolecular systems, *Chem. Rev.*, 2001, **101**, 4125–4155.
2 P.-H. Chien, K. J. Griffith, H. Liu, Z. Gan and Y.-Y. Hu, Recent Advances in Solid-State Nuclear Magnetic Resonance Techniques for Materials Research, *Annu. Rev. Mater. Res.*, 2020, **50**, 493–520.
3 T. K. Karamanos, A. P. Kalverda and S. E. Radford, Generating Ensembles of Dynamic Misfolding Proteins, *Front. Neurosci.*, 2022, **16**, 1–14.
4 D. L. Bryce, New frontiers for solid-state NMR across the periodic table: A snapshot of modern techniques and instrumentation, *Dalton Trans.*, 2019, **48**, 8014–8020.
5 S. E. Ashbrook, Solid-state NMR spectroscopy, *Phys. Chem. Chem. Phys.*, 2009, **11**, 6875.
6 R. W. Schurko, Ultra-wideline solid-state NMR spectroscopy, *Acc. Chem. Res.*, 2013, **46**, 1985–1995.
7 S. E. Ashbrook and S. Sneddon, New methods and applications in solid-state NMR spectroscopy of quadrupolar nuclei, *J. Am. Chem. Soc.*, 2014, **136**, 15440–15456.
8 A. Medek, V. Frydman and L. Frydman, Central Transition Nuclear Magnetic Resonance in the Presence of Large Quadrupole Couplings: Cobalt-59 Nuclear Magnetic Resonance of Cobaltophthalocyanines, *J. Phys. Chem. A*, 1999, **103**, 4830–4835.
9 D. Massiot, I. Farnan, N. Gautier, D. Trumeau, A. Trokiner and J. P. Coutures, ^{71}Ga and ^{69}Ga nuclear magnetic resonance study of beta-Ga_2O_3: resolution of four- and six-fold coordinated Ga sites in static conditions, *Solid State Nucl. Magn. Reson.*, 1995, **4**, 241–248.
10 C. P. Slichter, NMR Study of Platinum Catalysis, *Surf. Sci.*, 1981, **106**, 382–396.
11 T. J. Bastow, M. E. Smith and S. N. Stuart, Observation of ^{91}Zr NMR in zirconium-based metals and oxides, *Chem. Phys. Lett.*, 1992, **19**, 125–129.
12 T. J. Bastow and M. E. Smith, ^{91}Zr NMR characterisation of phases in transformation toughened zirconia, *Solid State Nucl. Magn. Reson.*, 1992, **1**, 165–174.
13 F. H. Larsen, J. Skibsted, H. J. Jakobsen and N. C. Nielsen, Solid-state QCPMG NMR of low-γ quadrupolar metal nuclei in natural abundance, *J. Am. Chem. Soc.*, 2000, **122**, 7080–7086.
14 F. H. Larsen, H. J. Jakobsen, P. D. Ellis and N. C. Nielsen, High-field QCPMG-MAS NMR of half-integer quadrupolar nuclei with large quadrupole couplings, *Mol. Phys.*, 1998, **95**, 1185–1195.
15 A. S. Lipton, M. D. Smith, R. D. Adams and P. D. Ellis, Zn solid-state and single-crystal NMR spectroscopy and X-ray crystal structure of zinc formate dihydrate, *J. Am. Chem. Soc.*, 2002, **124**, 410–414.
16 A. S. Lipton, R. W. Heck, M. Hernick, C. A. Fierke and P. D. Ellis, Residue ionization in LpxC directly observed by ^{67}Zn NMR spectroscopy, *J. Am. Chem. Soc.*, 2008, **130**, 12671–12679.
17 H. Nagashima, J. Trébosc, Y. Kon, K. Sato, O. Lafon and J. P. Amoureux, Observation of Low-γ Quadrupolar Nuclei by Surface-Enhanced NMR Spectroscopy, *J. Am. Chem. Soc.*, 2020, **142**, 10659–10672.
18 B. E. G. Lucier, K. E. Johnston, W. Xu, J. C. Hanson, S. D. Senanayake, S. Yao, M. W. Bourassa, M. Srebro, J. Autschbach and R. W. Schurko, Unravelling the structure of Magnus' pink salt, *J. Am. Chem. Soc.*, 2014, **136**, 1333–1351.
19 L. A. O'Dell and R. W. Schurko, QCPMG using adiabatic pulses for faster acquisition of ultra-wideline NMR spectra, *Chem. Phys. Lett.*, 2008, **464**, 97–102.
20 A. J. Rossini, R. W. Mills, G. A. Briscoe, E. L. Norton, S. J. Geier, I. Hung, S. Zheng, J. Autschbach and R. W. Schurko, Solid-state chlorine NMR of group IV transition metal organometallic complexes, *J. Am. Chem. Soc.*, 2009, **131**, 3317–3330.
21 D. Laurencin, F. Ribot, C. Gervais, A. J. Wright, A. R. Baker, L. Campayo, J. V. Hanna, D. Iuga, M. E. Smith, J. M. Nedelec, G. Renaudin and C. Bonhomme, ^{87}Sr, ^{119}Sn, ^{127}I Single and $\{^1H/^{19}F\}$-Double Resonance Solid-State NMR Experiments: Application to Inorganic Materials and Nanobuilding Blocks, *ChemistrySelect*, 2016, **1**, 4509–4519.
22 L. Piveteau, M. Aebli, N. Yazdani, M. Millen, L. Korosec, F. Krieg, B. M. Benin, V. Morad, C. Piveteau, T. Shiroka, A. Comas-Vives, C. Copéret, A. M. Lindenberg, V. Wood, R. Verel and M. V. Kovalenko, Bulk and Nanocrystalline Cesium Lead-Halide Perovskites as Seen by Halide Magnetic Resonance, *ACS Cent. Sci.*, 2020, **6**, 1138–1149.
23 D. L. Bryce and G. D. Sward, Solid-state NMR spectroscopy of the quadrupolar halogens: Chlorine-35/37, bromine-79/81, and iodine-127, *Magn. Reson. Chem.*, 2006, **44**, 409–450.
24 L. A. O'Dell, A. J. Rossini and R. W. Schurko, Acquisition of ultra-wideline NMR spectra from quadrupolar nuclei by frequency stepped WURST-QCPMG, *Chem. Phys. Lett.*, 2009, **468**, 330–335.
25 A. S. Lipton, J. A. Sears and P. D. Ellis, A general strategy for the NMR observation of half-integer quadrupolar nuclei in dilute environments, *J. Magn. Reson.*, 2001, **151**, 48–59.
26 C. M. Widdifield and D. L. Bryce, Solid-state ^{127}I NMR and GIPAW DFT study of metal iodides and their hydrates: Structure, symmetry, and higher-order quadrupole-induced effects, *J. Phys. Chem. A*, 2010, **114**, 10810–10823.
27 L. Müller, Sensitivity Enhanced Detection of Weak Nuclei Sensitivity Enhanced Detection of Weak Nuclei Using Heteronuclear Multiple Quantum Coherence, *J. Am. Chem. Soc.*, 1979, **101**, 4481–4484.
28 S. Cavadini, A. Abraham and G. Bodenhausen, Proton-detected nitrogen-14 NMR by recoupling of heteronuclear dipolar interactions using symmetry-based sequences, *Chem. Phys. Lett.*, 2007, **445**, 1–5.

Open Access Article. Published on 16 January 2024. Downloaded on 2/10/2026 6:49:38 PM. This article is licensed under a Creative Commons Attribution-NonCommercial 3.0 Unported Licence.

29 S. Cavadini, A. Lupulescu, S. Antonijevic and G. Bodenhausen, Nitrogen-14 NMR spectroscopy using residual dipolar splittings in solids, *J. Am. Chem. Soc.*, 2006, **128**, 7706–7707.
30 Z. Gan, Measuring amide nitrogen quadrupolar coupling by high-resolution $^{14}N/^{13}C$ NMR correlation under magic-angle spinning, *J. Am. Chem. Soc.*, 2006, **128**, 6040–6041.
31 Y. Nishiyama, Y. Endo, T. Nemoto, H. Utsumi, K. Yamauchi, K. Hioka and T. Asakura, Very fast magic angle spinning ^{1}H-^{14}N 2D solid-state NMR: Sub-micro-liter sample data collection in a few minutes, *J. Magn. Reson.*, 2011, **208**, 44–48.
32 S. Cavadini, S. Antonijevic, A. Lupulescu and G. Bodenhausen, Indirect detection of nitrogen-14 in solids via protons by nuclear magnetic resonance spectroscopy, *J. Magn. Reson.*, 2006, **182**, 168–172.
33 S. Cavadini, A. Abraham, S. Ulzega and G. Bodenhausen, Evidence for dynamics on a 100 ns time scale from single- and double-quantum nitrogen-14 NMR in solid peptides, *J. Am. Chem. Soc.*, 2008, **130**, 10850–10851.
34 M. Grüne, R. Luxenhofer, D. Iuga, S. P. Brown and A. C. Pöppler, ^{14}N-^{1}H HMQC solid-state NMR as a powerful tool to study amorphous formulations-an exemplary study of paclitaxel loaded polymer micelles, *J. Mater. Chem. B*, 2020, **8**, 6827–6836.
35 A. S. Tatton, T. N. Pham, F. G. Vogt, D. Iuga, A. J. Edwards and S. P. Brown, Probing hydrogen bonding in cocrystals and amorphous dispersions using ^{14}N-^{1}H HMQC solid-state NMR, *Mol. Pharm.*, 2013, **10**, 999–1007.
36 C. D. Makowka, C. P. Slichter and J. H. Sinfelt, NMR of platinum catalysts: Double NMR of chemisorbed carbon monoxide and a model for the platinum NMR line shape, *Phys. Rev. B: Condens. Matter Mater. Phys.*, 1985, **31**, 5663–5679.
37 C. D. Makowka, C. P. Slichter and J. H. Sinfelt, Probe of the Surface of a Heterogeneous Catalyst: Double NMR of Carbon Monoxide Chemisorbed on Highly Dispersed Platinum, *Phys. Rev. Lett.*, 1982, **49**, 379–382.
38 P. K. Wang, J. P. Ansermet, S. L. Rudaz, Z. Wang, S. Shore, C. P. Slichter and J. H. Sinfelt, NMR Studies of Simple Molecules on Metal Surfaces, *Science*, 1986, **234**, 35–41.
39 C. P. Grey and A. J. Vega, Determination of the Quadrupole Coupling Constant of the Invisible Aluminum Spins in Zeolite HY with $^{1}H/^{27}A1$ TRAPDOR NMR, *J. Am. Chem. Soc.*, 1995, **117**, 8232–8242.
40 M. Kalwei and H. Koller, Quantitative comparison of REAPDOR and TRAPDOR experiments by numerical simulations and determination of H-Al distances in zeolites, *Solid State Nucl. Magn. Reson.*, 2002, **21**, 145–157.
41 C. Schroeder, V. Siozios, C. Mück-Lichtenfeld, M. Hunger, M. R. Hansen and H. Koller, Hydrogen Bond Formation of Brønsted Acid Sites in Zeolites, *Chem. Mater.*, 2020, **32**, 1564–1574.
42 R. W. Dorn, B. J. Ryan, S. N. S. Lamahewage, M. V. Dodson, J. B. Essner, R. Biswas, M. G. Panthani and A. J. Rossini, Chlorination of Hydrogenated Silicon Nanosheets Revealed by Solid-State Nuclear Magnetic Resonance Spectroscopy, *Chem. Mater.*, 2023, **35**, 539–548.
43 N. T. Duong and Y. Nishiyama, Detection of remote proton-nitrogen correlations by ^{1}H-detected ^{14}N overtone solid-state NMR at fast MAS, *Phys. Chem. Chem. Phys.*, 2022, **24**, 10717–10726.
44 Z. Gan, Rotary resonance echo double resonance for measuring heteronuclear dipolar coupling under MAS, *J. Magn. Reson.*, 2006, **183**, 235–241.
45 C. P. Grey, W. S. Veeman and A. J. Vega, Rotational echo $^{14}N/^{13}C/^{1}H$ triple resonance solid-state nuclear magnetic resonance: A probe of ^{13}C-^{14}N internuclear distances, *J. Chem. Phys.*, 1993, **98**, 7711–7724.
46 A. Venkatesh, D. Gioffrè, B. A. Atterberry, L. Rochlitz, S. L. Carnahan, Z. Wang, G. Menzildjian, A. Lesage, C. Copéret and A. J. Rossini, Molecular and Electronic Structure of Isolated Platinum Sites Enabled by the Expedient Measurement of ^{195}Pt Chemical Shift Anisotropy, *J. Am. Chem. Soc.*, 2022, **144**, 13511–13525.
47 T. Wolf, A. Eden-Kossoy and L. Frydman, Indirectly detected satellite-transition quadrupolar NMR via progressive saturation of the proton reservoir, *Solid State Nucl. Magn. Reson.*, 2023, **125**, 101862.
48 M. J. Jaroszewicz, A. R. Altenhof, R. W. Schurko and L. Frydman, Sensitivity Enhancement by Progressive Saturation of the Proton Reservoir: A Solid-State NMR Analogue of Chemical Exchange Saturation Transfer, *J. Am. Chem. Soc.*, 2021, **143**, 19778–19784.
49 B. A. Atterberry, S. L. Carnahan, Y. Chen, A. Venkatesh and A. J. Rossini, Double echo symmetry-based REDOR and RESPDOR pulse sequences for proton detected measurements of heteronuclear dipolar coupling constants, *J. Magn. Reson.*, 2022, **336**, 107147.
50 M. Bak, J. T. Rasmussen and N. C. Nielsen, SIMPSON: A General Simulation Program for Solid-State NMR Spectroscopy, *J. Magn. Reson.*, 2000, **147**, 296–330.
51 Z. Tošner, T. Vosegaard, C. Kehlet, N. Khaneja, S. J. Glaser and N. C. Nielsen, Optimal control in NMR spectroscopy: Numerical implementation in SIMPSON, *J. Magn. Reson.*, 2009, **197**, 120–134.
52 Z. Tošner, R. Andersen, B. Stevensson, M. Edén, N. C. Nielsen and T. Vosegaard, Computer-intensive simulation of solid-state NMR experiments using SIMPSON, *J. Magn. Reson.*, 2014, **246**, 79–93.
53 T. L. Hwang, P. C. M. Van Zijl and M. Garwood, Fast Broadband Inversion by Adiabatic Pulses, *J. Magn. Reson.*, 1998, **133**, 200–203.
54 A. Pankowska, K. Kochalska, A. Łazorczyk, K. Dyndor, P. Kozioł, B. Zieńczuk, M. Toborek and R. Pietura, Chemical exchange saturation transfer (CEST) as a new method of signal obtainment in magnetic resonance molecular imaging in clinical and research practice, *Pol. J. Radiol.*, 2019, **84**, e147–e152.
55 A. Brinkmann and A. P. M. Kentgens, Proton-selective ^{17}O-^{1}H distance measurements in fast magic-angle-spinning solid-state NMR spectroscopy for the determination of hydrogen bond lengths, *J. Am. Chem. Soc.*, 2006, **128**, 14758–14759.
56 B. E. G. Lucier, A. R. Reidel and R. W. Schurko, Multinuclear solid-state NMR of square-planar platinum complexes Cisplatin and related systems, *Can. J. Chem.*, 2011, **89**, 919–937.

Open Access Article. Published on 16 January 2024. Downloaded on 2/10/2026 6:49:38 PM. This article is licensed under a Creative Commons Attribution-NonCommercial 3.0 Unported Licence.

57 S. G. J. van Meerten, W. M. J. Franssen and A. P. M. Kentgens, ssNake: A cross-platform open-source NMR data processing and fitting application, *J. Magn. Reson.*, 2019, **301**, 56–66.

58 D. Sarkar, R. W. Hooper, A. Karmakar, A. Bhattacharya, A. Pominov, V. V. Terskikh and V. K. Michaelis, Metal Halide Perovskite and Perovskite-like Materials through the Lens of Ultra-wideline $^{35}/^{37}$Cl NMR Spectroscopy, *ACS Mater. Lett.*, 2022, **4**, 1255–1263.

59 K. Sonogashira, Y. Tohda and N. Hagihara, A convenient synthesis of acetylenes: catalytic substitutions of acetylenic hydrogen with bromoalkenes, iodoarenes and bromopyridines, *Tetrahedron Lett.*, 1975, **50**, 4467–4470.

60 D. G. Cory and W. M. Ritchey, Suppression of Signals from the Probe in Bloch Decay Spectra, *J. Magn. Reson.*, 1988, **80**, 128–160.

61 B. E. G. Lucier, J. A. Tang, R. W. Schurko, G. A. Bowmaker, P. C. Healy and J. V. Hanna, Solid-state ^{65}Cu and ^{31}P NMR spectroscopy of bis(triphenylphosphine) copper species, *J. Phys. Chem. C*, 2010, **114**, 7949–7962.

62 J. A. Tang, B. D. Ellis, T. H. Warren, J. V. Hanna, C. L. B. Macdonald and R. W. Schurko, Solid-state ^{63}Cu and ^{65}Cu NMR spectroscopy of inorganic and organometallic copper(I) complexes, *J. Am. Chem. Soc.*, 2007, **129**, 13049–13065.

63 H. Yu, X. Tan, G. M. Bernard, V. V. Terskikh, J. Chen and R. E. Wasylishen, Solid-State 63Cu, 65Cu, and 31P NMR Spectroscopy of Photoluminescent Copper(I) Triazole Phosphine Complexes, *J. Phys. Chem. A*, 2015, **119**, 8279–8293.

64 C. J. Pickard and F. Mauri, All-electron magnetic response with pseudopotentials: NMR chemical shifts, *Phys. Rev. B: Condens. Matter Mater. Phys.*, 2001, **63**, 2451011.

65 S. J. Clark, M. D. Segall, C. J. Pickard Ii, P. J. Hasnip, M. I. J. Probert, K. Refson and M. C. Payne, First principles methods using CASTEP, *Z. Kristallogr.*, 2005, **220**, 567–570.

66 F. A. Perras and D. L. Bryce, Direct investigation of covalently bound chlorine in organic compounds by solid-state ^{35}Cl NMR spectroscopy and exact spectral line-shape simulations, *Angew. Chem., Int. Ed.*, 2012, **51**, 4227–4230.

67 A. M. Callegari and M. Boiocchi, Häggite from the Gambatesa mine, Liguria, Italy: a refinement of the crystal structure, *Neues Jahrb. Mineral., Abh.*, 2015, **192**, 33–38.

68 T. Maly, G. T. Debelouchina, V. S. Bajaj, K. N. Hu, C. G. Joo, M. L. Mak-Jurkauskas, J. R. Sirigiri, P. C. A. Van Der Wel, J. Herzfeld, R. J. Temkin and R. G. Griffin, Dynamic nuclear polarization at high magnetic fields, *J. Chem. Phys.*, 2008, **128**, 052211.

69 E. Nimerovsky and A. Goldbourt, Efficient rotational echo double resonance recoupling of a spin-1/2 and a quadrupolar spin at high spinning rates and weak irradiation fields, *J. Magn. Reson.*, 2010, **206**, 52–58.

70 E. Nimerovsky, R. Gupta, J. Yehl, M. Li, T. Polenova and A. Goldbourt, Phase-modulated LA-REDOR: A robust, accurate and efficient solid-state NMR technique for distance measurements between a spin-1/2 and a quadrupole spin, *J. Magn. Reson.*, 2014, **244**, 107–113.

71 B. A. Rosales, L. Men, S. D. Cady, M. P. Hanrahan, A. J. Rossini and J. Vela, Persistent Dopants and Phase Segregation in Organolead Mixed-Halide Perovskites, *Chem. Mater.*, 2016, **28**, 6848–6859.

72 F. Zhu, L. Men, Y. Guo, Q. Zhu, U. Bhattacharjee, P. M. Goodwin, J. W. Petrich, E. A. Smith and J. Vela, Shape evolution and single particle luminescence of organometal halide perovskite nanocrystals, *ACS Nano*, 2015, **9**, 2948–2959.

73 R. K. Harris, E. D. Becker, S. M. Cabral De Menezes, R. Goodfellow and P. Granger, NMR nomenclature. Nuclear spin properties and conventions for chemical shifts (IUPAC recommendations 2001), *Pure Appl. Chem.*, 2001, **73**, 1795–1818.

74 A. J. Rossini, R. W. Mills, G. A. Briscoe, E. L. Norton, S. J. Geier, I. Hung, S. Zheng, J. Autschbach and R. W. Schurko, Solid-state chlorine NMR of group IV transition metal organometallic complexes, *J. Am. Chem. Soc.*, 2009, **131**, 3317–3330.

75 B. M. Fung, A. K. Khitrin and K. Ermolaev, An Improved Broadband Decoupling Sequence for Liquid Crystals and Solids, *J. Magn. Reson.*, 2000, **142**, 97–101.

 This journal is © the Owner Societies 2024